

*Accepted for publication in The Astrophysical Journal*

## **LBDS 53W091: An Old, Red Galaxy at $z=1.552$ <sup>1</sup>**

Hyron Spinrad

Astronomy Department, University of California at Berkeley, CA 94720

Electronic Mail: spinrad@astro.berkeley.edu

Arjun Dey

NOAO/KPNO<sup>2</sup>, 950 N. Cherry Ave., P. O. Box 26732, Tucson, AZ 85726

Electronic Mail: dey@noao.edu

Daniel Stern

Astronomy Department, University of California at Berkeley, CA 94720

Electronic Mail: dan@astro.berkeley.edu

James Dunlop

Institute for Astronomy, Department of Physics and Astronomy

The University of Edinburgh, Edinburgh EH9 3HJ, UK

Electronic Mail: J.Dunlop@roe.ac.uk

John Peacock and Raul Jimenez

Royal Observatory, Edinburgh EH9 3HJ, UK

Electronic Mail: (J.Peacock,R.Jimenez)@roe.ac.uk

Rogier Windhorst

Department of Physics and Astronomy, Arizona State University, Tempe, AZ 85287-1504

Electronic Mail: raw@cosmos.la.asu.edu

### **ABSTRACT**

The weak radio source LBDS 53W091 is associated with a very faint ( $R \approx 24.5$ ) red ( $R - K \approx 5.8$ ) galaxy. Long spectroscopic integrations with the W. M. Keck telescope have provided an absorption-line redshift,  $z = 1.552 \pm 0.002$ . The galaxy has a rest frame ultraviolet spectrum very similar to that of an F6 V star, and a single-burst old stellar population that matches the IR colors, the optical energy distribution and the

---

<sup>1</sup>Based in large part on observations made at the W.M. Keck Observatory.

<sup>2</sup>The National Optical Astronomy Observatories are operated by the Association of Universities for Research in Astronomy under cooperative agreement with the National Science Foundation.

spectral discontinuities has a minimum age of 3.5 Gyr. We present detailed population synthesis analyses of the observed spectrum in order to estimate the time since the last major epoch of star formation. We discuss the discrepancies in these estimates resulting from using different models, subjecting the UV spectrum of M32 to the same tests as a measure of robustness of these techniques. The models most consistent with the data tend to yield ages at  $z = 1.55$  of  $\gtrsim 3.5$  Gyr, similar to that inferred for the intermediate-age population in M32. Depending upon the assumed Hubble constant and the value of  $\Omega_0$ , only certain cosmological expansion times are consistent with the age of LBDS 53W091; in particular, for  $\Omega_0 = 1$ , only models with  $H_0 \lesssim 45 \text{ km s}^{-1} \text{ Mpc}^{-1}$  are permitted. For  $H_0 = 50 \text{ km s}^{-1} \text{ Mpc}^{-1}$  and  $\Omega_0 = 0.2$ , we derive a formation redshift,  $z_f \geq 5$ .

*Subject headings:* cosmology: early universe – galaxies: redshifts – galaxies: evolution – radio continuum: galaxies – stellar populations – galaxies: individual: LBDS 53W091

## 1. Introduction

Finding distant galaxies and analyzing their starlight remains one of the only direct methods of studying the formation and evolution of galaxies. In particular, the reddest normal galaxies at high redshifts provide the best constraints on the earliest epochs of galaxy formation and evolution, since their color is most likely due to an aged stellar population. Several photometric and spectroscopic studies of galaxy evolution out to redshifts  $z \sim 1$  have discovered that the red galaxy population (which predominantly consists of early type E/S0 galaxies) evolves “passively” with time, i.e., by the gradual reddening and fading of the integrated starlight (e.g., Driver et al. 1995ab; Lilly et al. 1995; Rakos & Schombert 1995; Schade et al. 1995; Stanford et al. 1995, 1997a; Oke et al. 1996). In addition, the discovery of  $z \sim 1$  cluster galaxies with morphologies and rest frame colors similar to those of nearby ellipticals (e.g., Couch et al. 1994; Dressler et al. 1995; Dickinson 1996; Dickinson et al. 1997) suggests a high formation redshift ( $z > 2$ ) for the red population and emphasizes the importance of studying these objects at even larger lookback times.

The high-redshift red galaxy population is faint at observed optical (rest-frame ultraviolet) wavelengths, and therefore most studies of galaxies at high redshift have concentrated on the luminous, blue, emission line objects (star-forming and active galaxies) which are easier to find and relatively easy to study spectroscopically at optical wavelengths (e.g., Cowie et al. 1995, Steidel et al. 1996). One of the prerequisites to studying old populations at high redshifts is therefore to find distant luminous early type galaxies. The association of nearby, bright radio sources with low redshift giant elliptical and cD galaxies suggests that a good method of finding such old populations at high redshifts is to search for the optical counterparts of faint radio sources (Kron et al. 1985). This has been the primary driving force behind several radio source identification and redshift determination programs over the last three decades, and has resulted in several nearly completely

identified radio source catalogues (e.g., 3CR — Spinrad & Djorgovski 1987; Molonglo — McCarthy et al. 1996; 1Jy — Lilly 1989; Parkes — Dunlop et al. 1989a; 2Jy — Tadhunter et al. 1993; MG — Stern et al. 1997).

Unfortunately, most of these studies, although resulting in a large number of high-redshift objects, are of limited use for studying the evolution of normal galaxies. This is primarily because the ultraviolet (UV) light in most luminous radio galaxies is dominated by scattered light from and photoionization by the active nucleus rather than starlight (e.g., McCarthy et al. 1987; Chambers et al. 1987; di Serego Alighieri et al. 1989; di Serego Alighieri et al. 1994; Jannuzi & Elston 1991; Jannuzi et al. 1995; Dey & Spinrad 1996; Dey et al. 1996; Cimatti et al. 1996). Nevertheless, there have been several attempts to age-date the underlying stellar population using broad band optical and near-infrared photometry (e.g., Dunlop et al. 1989b; Chambers & Charlot 1990; McCarthy 1993) and a few valiant efforts using moderate signal-to-noise ratio spectroscopy (e.g., Stockton, Kellogg & Ridgway 1995; Chambers & McCarthy 1990). These attempts have been limited by the inherent ambiguities of modelling broad band colors and, in the spectroscopic studies, the problems of subtracting the strong emission lines and UV non-stellar continuum light and correctly decomposing the AGN and stellar components.

Although radio galaxies have been, thus far, of limited cosmological utility, they are not to be discarded as useful probes of the early epochs of galaxy formation and evolution. First, they are still the highest redshift galaxy-like objects (i.e., spatially extended and possibly composed of stars) known (e.g., Lacy et al. 1995; Spinrad, Dey & Graham 1995; Rawlings et al. 1996). Second, there appears to be a good correlation between radio power and the fractional contribution of non-stellar AGN light to the UV spectrum; in particular, weak radio sources ( $S_{1.4 \text{ GHz}} < 50 \text{ mJy}$ ) generally have very weak emission lines and, unlike the powerful radio galaxies, do not exhibit UV / radio alignments, suggesting that the contribution of scattered AGN emission to their continuum light is small (e.g., Rawlings & Saunders 1991; Dunlop & Peacock 1993; Eales & Rawlings 1993; Vigotti et al. 1996). Hence, *weak* radio sources with red optical / IR colors may *still* provide us with the ability of studying uncontaminated starlight in nearly normal, luminous elliptical galaxies at high redshift. The radio source selection above a few mJy almost guarantees an early type host galaxy (e.g., Dunlop, Peacock & Windhorst 1995 and references therein) and the near-IR magnitude and color criteria ensure that the galaxy will be at high redshift. For reference, a present-day  $L^*$  elliptical galaxy observed at a redshift  $z \approx 1$ , has a typical magnitude of  $K \approx 18.5$  and color ( $R - K \approx 6$ ).

In order to further test this hypothesis, we have chosen as targets for deep optical spectroscopy a subset of weak radio sources ( $1 \text{ mJy} < S_{1.4 \text{ GHz}} < 50 \text{ mJy}$ ) from the Leiden-Berkeley Deep Survey (hereinafter LBDS; Windhorst et al. 1984ab) which are associated with host galaxies that have faint near-IR magnitudes ( $K \geq 18$ ) and red optical-IR colors ( $R - K > 5$ ). Photometry is now available for a statistically complete sample of 77 galaxies having *griJHK* photometry to  $r \simeq 26$  and  $K \simeq 20$  (Dunlop, Peacock, & Windhorst 1995). In this paper, we present our results on LBDS 53W091, a weak radio source ( $S_{1.4 \text{ GHz}} \approx 20 \text{ mJy}$ ) which is among the reddest faint LBDS galaxies, suggesting a substantial distance and an aged population. Early results on this

galaxy have already been reported by us elsewhere (Dunlop et al. 1996), and the present work includes a more detailed description of our data, spectral analyses, and age-dating techniques. In § 2 we present our optical, IR and radio imaging photometry and optical spectroscopy. The redshift determination is described in § 3. The derived age estimates based on spectral synthesis model fitting and the differences between the various models are presented in §4. In § 5 we discuss the cosmological implications of finding such an old galaxy at high redshift.

## 2. Observations

### 2.1. Optical Identification, Radio Imaging and Astrometry

The optical counterpart of the radio source LBDS 53W091 was first identified on images of the field obtained using the Palomar 200" Hale Telescope. The Four-shooter CCD-array on the Hale Telescope was used in 1984 – 1988 to systematically image those mJy radio sources in the  $17^h+50^o$  LBDS field (Windhorst, van Heerde, & Katgert 1984; WHK) that were fainter than  $V \leq 23.5$  mag (i.e., sources not detected on the deep *UJFN* plates obtained with the KPNO 4-m Mayall Telescope; Windhorst, Kron, & Koo 1984; WKK). The Four-shooter imaging was done in Gunn *g* and *r*. Each frame consists of four simultaneously exposed  $800 \times 800$  TI CCDs, and covers  $\approx 9' \times 9'$ .

Details of the Four-shooter imaging, calibration, and reduction are given by Neuschaefer & Windhorst (1995a, b; NW95a, NW95b). This includes a careful removal of large scale gradients to within 0.1% of sky, so that aperture magnitudes could be reliably grown to total (see Windhorst et al 1991). Photometric calibration was done measuring standard stars from Thuan & Gunn (1976) and Kent (1985), and correcting for atmospheric extinction as a function of airmass and (*g* – *r*) color. From overlapping Four-shooter regions and multiple exposures during different observing runs, we could check the internal consistency of the photometry during these runs, which was usually  $\leq 0.08 - 0.1$  mag (NW95a). Astrometry was done with typically 30 primary standard stars from recent Palomar 48 inch Schmidt plates, and 6–8 standard stars in each Four-shooter CCD, as described by WKK and NW95a. With repeated astrometric measurements under different plate orientations, a global astrometric accuracy could be obtained of  $0''.3 - 0''.5$ . The Westerbork radio positions of WHK and the VLA positions of Oort et al. (1987) (with typical accuracies of  $0''.2 - 0''.3$ ) were sufficient to find a reliable optical identification for each source.

High resolution radio images of LBDS 53W091 at frequencies of 1.56 GHz and 4.86 GHz were obtained using the VLA A-array in snapshot mode on 1995 October 29. Figure 1 shows the 4.86 GHz map of the radio source, and the radio data are presented in Table 1. The source is a double-lobed FRII steep-spectrum ( $\alpha_{1.56 \text{ GHz}}^{4.86 \text{ GHz}} \approx 1.1$ ,  $S_\nu \propto \nu^{-\alpha}$ ) radio source. The radio lobes are separated by  $\approx 4''.3$  in position angle  $PA \approx 131^\circ$ .

The VLA A-array position of LBDS 53W091 is RA= $17^h 21^m 17^s.81 \pm 0^s.01$ , DEC= $+50^\circ 08' 47''.4 \pm 0''.1$  (B1950; Oort et al. 1987), and the best astrometric position for the optical candidate for

LBDS 53W091 is RA=17<sup>h</sup> 21<sup>m</sup> 17<sup>s</sup>84±0<sup>s</sup>03, DEC=+50° 08′ 47″7±0″3 (B1950; NW95a). Its optical fluxes result in magnitudes in Gunn  $g \geq 26.0$  ( $2\sigma$ ) and  $r = 25.10 \pm 0.15$  mag (see NW95a,b for details). Its 1.41 GHz radio flux density is  $22.4 \pm 0.9$  mJy from WSRT observations (with a beamsize of 12″ FWHM) in 1980–1984 (Windhorst et al. 1984, Oort & van Langevelde 1987). Its 0.61 GHz WSRT flux density is  $66.0 \pm 3.9$  mJy, implying a 0.61–1.41 GHz spectral index of  $1.30 \pm 0.13$ . The source is resolved at the 1.4″ FWHM VLA A-array resolution, and has LAS=4″2 ± 0″5 (Oort et al. 1987). The 1.490 GHz VLA A-array flux density measured in 1985, transformed back to 1.41 GHz with the measured spectral index, was  $S_{1.41} = 28.8 \pm 1.5$  mJy. The 1995 VLA A-array flux density, transformed to 1.41 GHz with the spectral index calculated from those observations, was  $S_{1.41} = 25.9 \pm 1.9$  mJy.

The VLA A-array observations were done at  $\sim 10\times$  higher resolution than the WSRT observations, and therefore may systematically miss flux. It is therefore curious that the 1985 VLA 1.41 GHz flux density is slightly higher (at the combined  $3.7\sigma$  level) than the 1980–1984 WSRT 1.41 GHz flux density, so that the possibility of *weak* nuclear variability cannot be ruled out. However, given its weak radio flux, steep-spectrum, and small but resolved angular size, the radio properties point at best to a relatively weak AGN. We note that the occurrence of a faint *red* identification for a compact weak radio source is quite common in the LBDS sample (cf. Kron et al. 1985, Windhorst et al. 1985), but less common in a  $\mu$ Jy sample (Windhorst et al. 1995).

## 2.2. Optical and Near-Infrared Imaging and Photometry

We obtained an  $R$ -band image of the field of LBDS 53W091 using the Low-Resolution Imaging Spectrometer (LRIS; Oke et al. 1995) on the W. M. Keck Telescope on UT 1995 July 25. The LRIS detector is a Tektronix 2048<sup>2</sup> CCD with 24  $\mu$ m pixels corresponding to a scale of 0″214 pixel<sup>-1</sup>. We obtained two 300s exposures under photometric conditions in fairly good seeing (the coadded image has FWHM<sub>PSF</sub>  $\approx 1''$ ). The images were bias-corrected and flat-fielded using a median image of the twilight sky. Photometric calibration was performed using observations of the standard field SA 113 (Landolt 1992). The coadded Keck  $R$  image is shown in Figure 2, and reaches a  $3\sigma$  limiting magnitude of 25.6 in a 4″ diameter aperture. A detail of this image centered on LBDS 53W091 is shown in Figure 3a.

Near-infrared images of LBDS 53W091 were obtained using the 3.9-m United Kingdom Infrared Telescope (UKIRT). On UT 1993 May 16 we obtained a 54-minute  $K$ -band image using the  $62 \times 58$  pixel InSb array camera IRCAM1, with the camera operating in the 0.62 arcsec pixel<sup>-1</sup> mode. Deep  $J$ -band (54 minutes) and  $H$ -band (81 minutes) images of LBDS 53W091 were subsequently obtained on UT 1995 August 19 using the  $256 \times 256$  pixel InSb array camera IRCAM3, with an image scale of 0.286 arcsec pixel<sup>-1</sup>. The infrared images were constructed from a mosaic of short-exposure ( $< 3$  minutes) frames which were shifted with respect to each other by between 8 and 15 arcsec. This procedure meant that the target source fell on a different set of pixels in each frame, and so the frames could be median filtered to provide an accurate sky flat-field for the image

concerned. The reduction procedure was as follows: (i) subtraction of a dark/bias frame from each sub-image; (ii) removal of known bad pixels; (iii) scaling of each image to the same median level, followed by median filtering of the stack; (iv) normalization of the resulting flat field; (v) division of each sub-image by the flat-field; (vi) construction of the final mosaic involving accurate registration, subtraction of frame-to-frame DC variations, and averaging of regions of overlap. The resulting mosaiced images reach  $3\sigma$  detection limits of  $\mu_K \simeq 21$  mag arcsec $^{-2}$ ,  $\mu_H \simeq 22$  mag arcsec $^{-2}$  and  $\mu_J \simeq 23.5$  mag arcsec $^{-2}$ . A detail of the  $J + H$  image is presented in Figure 3b, and the optical and near-infrared photometry are presented in Table 2.

Figure 4 (Plate 1) shows a false-color composite of the field constructed using the  $R$ ,  $J$  and  $H$  images. There are three red compact objects that appear to be in a close group near the center of the field. LBDS 53W091 is associated with the western-most and brightest red object in the central triad, and is clearly one of the reddest objects in the field, with  $(R - K) \approx 5.8$  (Table 2). The two galaxies that lie immediately to the NE and SE of LBDS 53W091 appear to have similar colors and may be companion galaxies. The two blue galaxies that lie near LBDS 53W091 (labelled “1” and “3b” in Figure 3) are both foreground emission line systems as described below.

Our images show that the three red galaxies are marginally resolved (seeing deconvolved FWHM  $\approx 0''.5 - 0''.7$ ), and the images are consistent with the galaxies being symmetric. More detailed comments on the rest frame UV and optical morphologies await observations with the *Hubble Space Telescope* (*HST*).

### 2.3. Spectroscopy

We observed LBDS 53W091 at the Cassegrain focus of the 10-m W. M. Keck Telescope using LRIS in May, July, August and September 1995. We used a 300 line/mm grating ( $\lambda_{\text{blaze}} = 5000\text{\AA}$ ) to cover the wavelength region  $\lambda\lambda 4000 - 9500\text{\AA}$  and a  $1''$  slit which resulted in a resolution FWHM  $\approx 10\text{\AA}$ . The data from UT 1995 July 25, August 31 and September 1 were of the best quality: the galaxy was detected in all these individual spectra and the seeing varied between  $0''.8$  and  $1''.0$  during the observations. These observations were all made with the slit oriented at position angle  $PA = 126^\circ$  in order to obtain spectra of the two brightest red objects in the field, LBDS 53W091 and galaxy 3a (e.g., Dunlop et al. 1996). On these nights, the parallactic angle varied between  $95^\circ$  and  $150^\circ$ , and our relative spectrophotometry should not be adversely affected by atmospheric refraction.

The data were bias-corrected, and flat-fielded using internal quartz flats obtained immediately after each observation. These observations of LBDS 53W091, galaxy 3a and 3b (see Figure 3 for nomenclature) were extracted using apertures of  $1''.7$  (8 pixels). The individual spectra were wavelength calibrated using HgKr and NeA lamps obtained after each observation. Flux calibration was performed using, on different nights, observations of the standard stars Feige 110, BD+33 $^\circ$ 2642, G191B2B and Wolf 1346. Standard star spectra were obtained both with and without a GG495

order-blocking filter in order to correct for the second order light at long wavelengths. The flux calibrated spectra of LBDS 53W091 from different nights are consistent with each other: the average flux in the wavelength region from 6500Å to 8500Å showed night-to-night variations of less than 15%. Finally, the individual spectra of LBDS 53W091 were corrected for the effects of telluric O<sub>2</sub> absorption using an absorption template determined from the observations of the standard stars and scaled to the appropriate airmass. The corrected spectra were then coadded to produce the final spectrum shown in Figure 5. The resultant spectrogram has an effective exposure time of 5.5 hours.

The two red galaxies (LBDS 53W091 and 3a) have similar spectra and similar  $R - K$  colors, although the data for LBDS 53W091 are of higher signal-to-noise ratio. In Figure 6 we present binned spectra of galaxy 3a and LBDS 53W091 to illustrate their similarities; note, in particular, the continuum discontinuity at 7400Å. The spectra of the two blue galaxies (“1” and “3b”) are shown in Figure 7. Galaxy 1, which lies 5".5 NW of LBDS 53W091, shows moderately strong [O II]λ3727 emission and Mg II absorption at  $z = 1.105$  (the Mg II absorption is affected by telluric Na D emission). The fainter galaxy 3b has two weak emission lines at 5185Å and 6964Å which we identify as [O II]λ3727 and [O III]λ5007 at  $z \approx 0.4$ . Table 3 lists their emission line identifications, fluxes and redshifts. The spectrum shown of galaxy 1 represents 1 hour of integration on UT 95 May 27; galaxy 3b was observed along the same long slit as LBDS 53W091 and thus represents 5.5 hours of total integration.

### 3. Results

#### 3.1. Redshift Determinations

As mentioned above, the bluer galaxies (1 and 3b) have emission line spectra and are moderately low redshift galaxies similar to those found in deep field surveys (e.g., Lilly et al. 1995; Cowie et al. 1995). It is the interpretation of the two *red* galaxies with absorption line spectra (LBDS 53W091 and 3a) that are the crux of this paper, and therefore the remainder of this section describes the determination of their redshifts.

The key to understanding the spectrum of LBDS 53W091 is the unique “tophat”-shaped region that is observed near  $\lambda\lambda 6740 - 7000 \text{ \AA}$  (see Figure 5). Inspection of the ultraviolet spectra of F and G dwarfs obtained with the *Copernicus* and *International Ultraviolet Explorer (IUE)* satellites clearly show a similarly shaped feature commencing at rest wavelength  $\lambda_0 2640 \text{ \AA}$  (e.g., Morton et al. 1977; Wu et al. 1991; Figure 8). This tophat feature is caused by metal line-blanketing on either side: in Solar type stars, the short wavelength edge is defined largely by Fe II absorption lines, and the continuum depression on the long wavelength side is dominated by the several weak metal lines and two strong absorption features of Mg IIλ2800Å and Mg Iλ2852Å (in individual spectra of G2V stars the equivalent width of the Mg II doublet is more than 25Å; Morton et al. 1977, Fanelli et al. 1992). We note that the observed dip in the spectrum of LBDS 53W091 at  $\lambda_{obs} \approx 6913\text{\AA}$

coincides with a blended (and therefore broad) telluric OH feature. The errors in the spectrum in this wavelength region are large and the galaxy faint, and we do not place much weight on this particular narrow absorption feature. However, if this feature is indeed real, it is likely due to Mg II $\lambda$ 2800 absorption arising in a foreground system at  $z \approx 1.47$  rather than a spectral feature associated with LBDS 53W091.

The overall shape of the observed continuum spectrum and the good match of the continuum breaks at  $\lambda_{\text{obs}} \approx 6735\text{\AA}$  and  $\approx 7500\text{\AA}$  with the known  $2640\text{\AA}$  and  $2900\text{\AA}$  spectral breaks, and the identification of the absorption feature at  $\lambda_{\text{obs}} \approx 7145\text{\AA}$  with the Mg II $\lambda$ 2800 $\text{\AA}$  doublet together suggest that the redshift of LBDS 53W091 is  $\approx 1.55$ . Cross correlation of the LBDS 53W091 spectrum in the rest wavelength range  $\lambda\lambda 2100 - 3080\text{\AA}$  with the spectrum of an F6V star from the Wu et al. (1991) *IUE* Spectral Atlas results in a more accurate redshift of  $1.552 \pm 0.002$ . The spectrum of LBDS 53W091 is also very similar to the spectra of two nearby elliptical galaxies, M32 and NGC 3610 (Figure 9); this comparison adds further confidence to our redshift determination. Finally, we have discovered several other galaxies with similar rest-frame spectra (Dey et al. 1997, Dickinson et al. 1997, Stanford et al. 1997b). All of these galaxies are at slightly lower redshifts; in several [O II] $\lambda$ 3727 emission and the Ca II H&K absorption lines are also detected, reinforcing the redshift determination from the  $2640\text{\AA}$  and  $2900\text{\AA}$  breaks. With the exception of one object, these other galaxies are not known to be radio sources, supporting the conclusion that these spectral features are due to starlight.

The spectrum of the fainter red galaxy 3a (Figure 6) is noisy at short wavelengths; nevertheless we can use the broad-band colors and the observed continuum discontinuity at  $7400\text{\AA}$  (which is very similar to the rest-frame  $2900\text{\AA}$  feature observed in LBDS 53W091) to derive an estimate of its redshift. The similarity in all the measured broad-band colors (Table 2) and the detection of the  $2900\text{\AA}$  break suggest similar redshifts for the two galaxies, and we therefore tentatively estimate  $z \approx 1.55$  for galaxy 3a. We note that galaxy 4 also has similar colors to LBDS 53W091 (although the errors are larger), and may therefore also be at a similar redshift.

### 3.2. LBDS 53W091 as a Radio Galaxy

LBDS 53W091 is a double-lobed FR II radio source and has a radio power at rest-frame 1.41 GHz of  $7.94 \times 10^{33} h_{50}^{-2} \text{ erg s}^{-1} \text{ Hz}^{-1}$ . Hence, although the radio power of LBDS 53W091 is at least 50 times less than that of the 3CR radio galaxies at similar redshifts, it is nevertheless a fairly powerful, steep-spectrum radio source that lies above the break in the radio galaxy luminosity function (e.g., Fanaroff & Riley 1974). In this subsection we discuss LBDS 53W091 in the context of two properties of powerful radio galaxies: the alignment effect and the uniformity of the  $K$  Hubble diagram. Both of these properties are relevant to our later discussion on the stellar content and age of LBDS 53W091.

The intriguing aspect of the spectrum of LBDS 53W091 is that it appears to be so similar to



that of nearby normal early-type galaxies. Most high-redshift powerful radio galaxies have rest-frame UV spectra that are dominated by strong line emission and non-stellar continuum emission. The spectrum of LBDS 53W091 shows no detectable emission lines. [O II] $\lambda$ 3727, usually the strongest feature in the optical window for galaxies in the redshift range  $z \approx 1.5$ , is redshifted to the very edge of our observed spectral range which is strongly contaminated by telluric OH emission. As a result, no useful limit can be placed on the [O II] line flux. We searched for possible weak UV emission lines of C II] $\lambda$ 2326 and C III] $\lambda$ 1909; none were found ( $5\sigma$  limits are  $f_{\text{CII]}}, f_{\text{CIII]}} \lesssim 3.2 \times 10^{-18} \text{ erg s}^{-1} \text{ cm}^{-2}$  in the observed frame) although they would be anticipated if an active nucleus contributed an appreciable flux of ionizing photons at shorter wavelengths. The lack of strong emission lines in the spectrum of LBDS 53W091 may very well be related to its lower radio luminosity. For example, deep spectroscopy of  $z \sim 1$  powerful radio sources (e.g., Stockton et al. 1996, Dey & Spinrad 1996) has demonstrated the presence of an underlying red stellar population that is veiled by the strong AGN-related UV emission in the rest-frame UV and only begins to dominate the spectrum at red rest-frame optical wavelengths. In radio galaxies containing lower luminosity AGN, it is therefore quite reasonable to expect that the diluting AGN continuum is lower, and that the starlight is more easily visible, and may even dominate the rest-frame UV spectrum.

The more powerful 3CR radio galaxies at similar redshifts ( $1 < z < 2$ ) also show very complex, elongated rest-frame UV morphologies that tend to be aligned with their radio axes, an indication that their morphologies are strongly influenced by the presence of the active nucleus (McCarthy et al. 1987, Chambers et al. 1987). The discovery that the extended UV continuum structures in many  $z > 0.7$  powerful radio galaxies are polarized has led to the suggestion that the aligned morphologies are caused by anisotropic radiation scattering off dust and electrons in the ambient medium into our line of sight (e.g., di Serego Alighieri et al. 1989). However, it has also been suggested that the aligned UV emission is starlight from a young stellar population formed by the expansion of the radio source into the dense ambient medium (De Young 1981, 1989, Begelman & Cioffi 1989). Whichever process is responsible, the relevant issue is whether or not one can consider the optical light from radio galaxies as being unaffected by the presence of the active nucleus, and therefore whether any conclusions regarding the evolution of radio galaxies may be generally extrapolated to the (luminous) early-type galaxy population as a whole.

If we consider galaxy 3a to be part of the LBDS 53W091 system, then it might be argued that LBDS 53W091 exhibits the alignment effect; i.e., the position angle of the axis connecting the host galaxy of the radio source to the companion galaxy 3a ( $PA \approx 126^\circ$ ) is roughly similar to that of the radio axis ( $PA \approx 130^\circ$ ). Since the UV spectra of both galaxies appear to be dominated by starlight, it is conceivable that the alignment in this system is the result of radio source triggered star formation. However, this seems unlikely given that both galaxies appear to be dominated by *old*, red populations, whereas the radio source is fairly compact ( $\approx 45$  kpc) and therefore likely young [ $\approx 4.4 \times 10^6 (v_{\text{expansion}}/10^4 \text{ km s}^{-1})^{-1} \text{ yr}$ ]. It is therefore more probable that the observed alignment is a chance coincidence. We also note that some alignments may result from anisotropic

infall along large-scale filaments and the possible alignments observed between these filaments and radio jet axes (e.g., West 1991).

Furthermore, the rest-frame UV spectrum argues against any significant scattered component: the flux is roughly zero at  $\lambda_{rest} \approx 1900\text{\AA}$  and  $2500\text{\AA}$ , and suggests that any significant scattered AGN component would have to be at least as red as the overall galaxy spectrum. If a reddened AGN spectrum is indeed present and dust-scattered as is the case in most of the luminous  $z \sim$  radio galaxies, we may expect to see a wavelength-dependent image structure: there is no evidence for this in LBDS 53W091. Finally, as discussed below, the  $2640\text{\AA}$  and  $2900\text{\AA}$  breaks are stellar absorption features and their amplitudes are reddening independent; the contribution of a highly reddened AGN component does not affect the inferences derived from these breaks regarding the age of the underlying stellar population.

It is well established that the  $K$  Hubble diagram of powerful radio galaxies shows remarkably little scatter ( $\sigma \sim 0.5$  mag) around a fairly linear  $K$ - $\log(z)$  relation (Lilly & Longair 1984, Lilly 1989, Eales et al. 1993). The  $K - z$  sequence may be well-represented by the predicted evolution of a passively evolving massive galaxy with a high formation redshift. LBDS 53W091 has a  $K$  magnitude of  $18.75 \pm 0.05$  and is therefore roughly 3 times brighter than an  $L^*$  ( $M_B = -21.0$ ) unevolved elliptical galaxy. Note that a population formed in an instantaneous burst at  $z = 5$  and evolving passively in an  $H_0=50 \text{ km s}^{-1} \text{ Mpc}^{-1}$ ,  $\Omega_0 = 0.2$  Universe will be  $\approx 1$  mag brighter in the  $K$  band at  $z \approx 1.55$  than an unevolved elliptical. LBDS 53W091 is therefore a galaxy whose local luminosity approximates that of an  $L^*$  galaxy. Using the SED of a 3.5 Gyr old population (from the Jimenez synthesis models; see § 4.3) to calculate the  $K$ -correction, we find rest-frame luminosities of  $M_K \approx -27.0$  and  $M_V \approx -23.9$  (for  $H_0=50 \text{ km s}^{-1} \text{ Mpc}^{-1}$ ,  $\Omega_0 = 0.2$ ).

Although LBDS 53W091 is roughly 2 times fainter ( $\approx 0.75$  mag) than the *mean* radio galaxy  $K - z$  relation (as determined from the 3CR and 1Jy sources), it still lies within the scatter of the Hubble diagram. Given that the  $K$ -band morphology of the radio galaxy appears undisturbed and consistent with that of an elliptical galaxy, we conclude that the AGN contributes little light, if any, in the observed  $K$ -band.

#### 4. Age-Dating the UV Population in LBDS 53W091

The similarity of the spectrum of LBDS 53W091 to the spectra of F and G stars (Figure 8) and, in particular, to the spectra of nearby old elliptical galaxies (Figure 9), suggests that this galaxy may serve as a high-redshift benchmark in the study of the evolution of early type galaxies. At a redshift of 1.55, an  $H_0=75 \text{ km s}^{-1} \text{ Mpc}^{-1}$ ,  $\Omega_0 = 1$ ,  $\Lambda = 0$  universe is only 2.1 Gyr old; hence, in principle, the age of the stellar population in LBDS 53W091 can place strong constraints on the cosmological parameters.

In this section we employ various methods to estimate the time elapsed since the last major epoch of star formation in LBDS 53W091. For the sake of conciseness, we refer to this time as

the ‘age’ of the stellar population. It is important to note that this age refers to the most recent star formation episode which currently dominates the UV spectrum, and *not* the first epoch of star formation in the galaxy. Determination of the age of the UV population therefore provides a *lower limit* to the age of the galaxy; the latter should include an additional time period for the dynamical assembly of the galaxy and the first epoch(s) of star formation (necessary to create the observed metals and mix them into the star forming material).

It is well known that the various extant evolutionary spectral synthesis models result in different ages when fit to the same optical spectra. These differences between the models are largely due to the differing treatments of stars in their post–main–sequence stages (cf. Charlot, Worthey, & Bressan 1996) as well as differing treatments of (main–sequence) stellar spectra in the UV. We therefore begin our analysis of the UV spectrum by deriving simple estimates of the age which are based solely on a determination of the color of the main–sequence turnoff population (§ 4.1 and 4.3) and comparisons to the UV spectra of nearby elliptical galaxies (§ 4.2). Age estimates based on the evolutionary synthesis models are presented in § 4.4. We also investigate the robustness of these age estimates by applying the same models to the UV spectrum of M32. Since the present spectrum of LBDS 53W091 is of insufficient signal-to-noise ratio for a detailed comparison with the spectral synthesis models, the UV color index  $R_{UV}$  and the break amplitudes  $B(2640)$  and  $B(2900)$  defined below provides a better alternative than spectral fitting for estimating the age of the stellar population.

#### 4.1. The Spectral Type of the Main-Sequence Turnoff Population: A Semi-Empirical Approach

The rest frame UV emission from a simple stellar population which is older than approximately 1 Gyr is dominated by starlight from the main–sequence turnoff population (e.g., Charlot & Bruzual 1991; S. Charlot, personal communication). For example, Figure 10 shows the spectrum of a 4 Gyr–old simple stellar population (constructed using the Jimenez et al. (1997) synthesis models described in § 4.4.4) subdivided into its various stellar evolutionary constituents, and clearly demonstrates that the main–sequence stars completely dominate the mid-UV flux at this age. Hence, the determination of the effective spectral type of the integrated UV light from the galaxy provides a fairly straightforward measure of the mean effective temperature of the turnoff population, and therefore an estimate of the time since the last epoch of star formation in the galaxy. In an attempt to derive a purely empirical age estimate for LBDS 53W091 in this section, we ignore for the present the small contributions to the UV light from evolved stars and stars below the main–sequence turnoff.

In order to evaluate the age of the stellar population of LBDS 53W091, we first compared its rest frame UV spectrum ( $\lambda\lambda_{\text{rest}}1800 - 3500$ ) to that of F and G stars observed by *IUE* (Wu et al. 1991; kindly made available to us by Yong Li and Dave Burstein) and to the Morton et al. (1977) spectrum of  $\alpha\text{CMi}$  (Procyon; F5IV — V) observed with *Copernicus*. We constructed “mean spectra” of main–sequence spectral types F0V, F2-3V, F5V, F6V, F7V, F9V, G0V, G2V,

G5V and G8V by averaging together the *IUE* spectra of the stars in these spectral type bins. The mean spectrum of type F6V provided the best fit to the spectrum of LBDS 53W091 and was able to reproduce the overall shape of the spectrum fairly accurately (Figure 8). This implies a color of  $(B - V) \approx 0.45$  for the main-sequence turnoff population.

In order to obtain an independent estimate of the best-matching spectral type which depends more on the details of the absorption spectrum than on the overall shape, we define two spectral breaks,  $B(2640)$  and  $B(2900)$ , at the 2640Å and 2900Å continuum discontinuities

$$B(2640) \equiv \frac{\bar{F}_\lambda(2645 - 2675\text{Å})}{\bar{F}_\lambda(2600 - 2630\text{Å})}$$

$$B(2900) \equiv \frac{\bar{F}_\lambda(2915 - 2945\text{Å})}{\bar{F}_\lambda(2855 - 2885\text{Å})},$$

and a longer wavelength baseline UV color index

$$R_{UV} \equiv \frac{\bar{F}_\lambda(3000 - 3200\text{Å})}{\bar{F}_\lambda(2000 - 2200\text{Å})}$$

where  $\bar{F}_\lambda(\lambda_1 - \lambda_2)$  is the average flux density (in  $\text{erg s}^{-1} \text{cm}^{-2} \text{Å}^{-1}$ ) in the wavelength interval  $[\lambda_1, \lambda_2]$ . Note that our definition of the break amplitudes differs slightly from that utilized in Dunlop et al. (1996).

Since the  $B(2640)$  and  $B(2900)$  breaks are defined over a narrow spectral range (as indicated in Figure 9), they are largely independent of reddening, and are determined primarily by the opacities of the metal absorption lines responsible for the absorption on their violet sides. Table 4 presents the measured break amplitudes for LBDS 53W091 and compares them with those determined from the mean F and G star spectra (see also Figures 11 and 12). It is important to note that the *IUE* spectra have reseau marks that contaminate the spectral regions  $\Delta\lambda \approx 2642 - 2650$  and  $\Delta\lambda \approx 2846 - 2856$  (Wu et al. 1991). These contaminate the flux at the blue edge of the tophat feature and the Mg I $\lambda$ 2852 absorption line. Since the tophat is roughly flat in this region, the  $B(2640)$  break determination remains unaffected. In addition, our definition of  $B(2900)$  starts just longward of the second affected region, and therefore this break is also fairly well determined.

Figures 11 and 12 show the variation of the  $B(2640)$  and  $B(2900)$  break amplitudes with color for main sequence stars in the *IUE* spectral atlas of Wu et al. (1991). The  $B(2640)$  break amplitude shows a significant scatter in the spectra of stars with spectral types later than F5V, and therefore can only provide a lower limit to the turnoff color of the UV population in LBDS 53W091 of  $(B - V)_{TO} \gtrsim 0.4$  (i.e., spectral types later than F5V). The  $B(2900)$  break amplitude shows smaller scatter with spectral type or  $(B - V)$  color, and therefore provides a more robust estimate on the color of the turnoff population of  $0.55 < (B - V)_{TO} < 0.75$  (i.e., spectral types F9V – G8V).

We determined stellar age estimates as a function of metallicity and turnoff color using the Revised Yale Isochrones (Green, Demarque and King 1987). The results of this analysis are tabulated in Table 5. For Solar metallicities ( $Z_\odot$ ) the bluest turnoff color ( $B - V \approx 0.45$ ) implies a

minimum age around 2.5 Gyr. If the true turnoff color is  $(B - V) \approx 0.6$  (as suggested by  $B(2900)$ ), then the corresponding turnoff age for a Solar abundance population is  $\approx 5$  Gyr.

The UV color index  $R_{UV}$  also results in a consistent estimate of the turnoff color. Figure 13 shows the variation of the UV color index with  $(B - V)$  color for the stars in the *IUE* spectral atlas. The UV color for LBDS 53W091 corresponds to a turnoff  $(B - V)$  color between 0.45 and 0.55 (typical of F5V – F9V stars) and implies a minimum age of  $\gtrsim 2.5$  Gyr for Solar metallicity populations. Note that the  $(B - V)$  color (and therefore age) remains roughly constant for values of the UV color index  $3.5 \lesssim R_{UV} \lesssim 10$  (corresponding to ages  $\sim 2.5 - 5$  Gyr). This index, along with the spectral breaks, provides a firm lower limit to the age of the composite population. The breaks and the overall spectrum, considered together, imply a turnoff color of  $(B - V) \gtrsim 0.45$  (spectral type later than F6V), with a best fit to the break amplitudes for  $(B - V) \sim 0.6$  (spectral type G0V). It is important to note that  $R_{UV}$  is more vulnerable than the spectral breaks to reddening by dust. The consistent estimates of the turnoff color determined from  $R_{UV}$  and the break amplitudes therefore reinforce our assumption that reddening due to dust is minimal.

The  $B(2640)$  and  $B(2900)$  breaks we define above are similar to the 2609/2660 and 2828/2921 spectral breaks defined by Fanelli et al. (1992). Studying the *IUE* spectra of a small sample of metal rich and metal poor stars, Fanelli et al. found that the strengths of these breaks are relatively insensitive to metallicity. For LBDS 53W091, we estimate these breaks (using the Fanelli et al. definition) to be  $0.97 \pm 0.24$  mag and  $0.64 \pm 0.15$  mag respectively. These values are typical of stars with  $(B - V) \approx 0.5 - 0.6$  (of spectral type F6V-G0V), and imply turnoff ages of  $\gtrsim 2.5$  Gyr for populations with  $Z \leq Z_{\odot}$ .

#### 4.2. Comparison with Nearby Elliptical Galaxies

As an additional empirical method to estimate the age of LBDS 53W091, it is instructive to directly compare the spectrum of LBDS 53W091 to the UV spectra of well-studied nearby galaxies in an attempt to determine an age *relative* to the local evolved galaxy population. The youngest stars in a galaxy will be the bluest, and therefore any young or intermediate-age population present will dominate the galaxy’s UV spectrum. In Figure 9 we plot the normalized rest-frame UV spectral energy distribution of LBDS 53W091 along with the *IUE* spectrum of M32 (Burstein et al. 1988) and the *HST* spectrum of NGC 3610 (Ferguson, private communication).

M32 is a nearby low luminosity galaxy which is believed to contain an intermediate-age stellar population ( $\sim 4 - 5$  Gyr old) in addition to the very old ( $\sim 10$  Gyr) stars usually present in elliptical galaxies (e.g., Baum 1959, O’Connell 1980, Burstein et al. 1984, Rocca-Volmerange & Guiderdoni 1987). Early studies of resolved stars in M32 (Freedman 1992, Elston & Silva 1992) and more recent studies of the integrated optical and ultraviolet spectrum (Bressan et al. 1994, Worthey 1994) are in good agreement with this conclusion, and imply that the most recent episode of star formation in M32 occurred 4 – 5 Gyr ago. In contrast, a recent deeper imaging study with *HST* by Grillmair

et al. (1996) finds that the red giant branch in M32 shows a substantial spread in color, implying that the galaxy also exhibits a substantial range in metallicity which will affect the interpretation of the UV light (i.e., the age of the younger population). Nevertheless, the youngest populations in M32 appear to have an age of  $\sim 4$  Gyr.

NGC 3610 is another well-studied nearby elliptical galaxy which shows evidence for the presence of an intermediate-age stellar population. NGC 3610 has an interesting morphology with twisted isophotes and a kinematically distinct core (Scorza & Bender 1990, Rix & White 1992), and shows evidence for a central stellar ring (Silva and Bothun 1997). The galaxy colors are bluer and the nucleus shows stronger  $H\beta$  absorption than similar  $M_B$  ellipticals, though the absorption is less than what is observed for E+A galaxies. Furthermore, the  $H - K$  color increases at the nucleus, a behavior opposite to what one expects from dust extinction, implying an extended AGB population because AGB stars are redder than RGB stars. Taken together, this evidence convincingly supports the existence of an intermediate-age population in NGC 3610 (Silva & Bothun 1997) similar to the more extensively studied case of M32. A comparison of the break amplitudes and the  $R_{UV}$  color index in NGC 3610 and M32 with those of late F and early G stars (Table 4) strongly supports the hypothesis that an intermediate-age population dominates the near-UV spectra in these galaxies.

In order to compare the overall shape of the spectra, we also defined broad spectral bins (in the ranges  $2200 - 2400\text{\AA}$ ,  $2650 - 2750\text{\AA}$ , and  $2900 - 3100\text{\AA}$ ) and determined crude color indices. We note that although M32 and NGC 3610 have composite stellar populations, the UV light in these galaxies is very likely to be dominated by the youngest turnoff population; the UV spectra of these galaxies therefore mimic that of a single burst populations, and the comparison to LBDS 53W091 is therefore justified. The spectrum of LBDS 53W091 is bluer than the spectra of both M32 and NGC 3610, suggesting that the last epoch of star formation in LBDS 53W091 may be slightly younger than that in these nearby galaxies, or alternatively that LBDS 53W091 has an additional source of UV continuum emission (cf. § 4.9). Although the UV continuum of LBDS 53W091 is bluer than that of M32 and NGC 3610, it is important to note that within the formal errors the amplitudes of the  $2640\text{\AA}$  and  $2900\text{\AA}$  breaks are roughly similar to these systems. We therefore estimate a minimum age of  $\sim 4$  Gyr for LBDS 53W091 based upon comparison with the near-UV spectra of nearby elliptical galaxies.

### 4.3. Main-Sequence Models

In § 4.1 we fit the UV spectrum of the integrated light from LBDS 53W091 with the spectrum of a single star. In this section, we make an attempt to fit the spectrum with a composite stellar population. In the present approximation, we synthesize the spectrum using a series of *main-sequence* stellar models. This approach assumes that the UV emission from the galaxy is composed entirely of starlight from main-sequence stars at and below the main-sequence turnoff. This ignores the contribution of subgiants and giants (the population just above the turnoff), but the impact of

these stars on the near-UV spectrum of a fairly old ( $\gtrsim 1\text{Gyr}$ ) population should be minimal, with almost all of the  $\sim \lambda 2700\text{\AA}$  light arising near the main-sequence turnoff point (Charlot, personal communication; see also Figure 10).

Employing the stellar atmosphere models of Kurucz (1992) and a Miller and Scalo (1979) initial mass function (IMF), we determined the spectral energy distribution for composite populations of different ages by integrating the light from the total main-sequence population (i.e., from the turnoff mass to the lower mass cutoff of the IMF). We computed the models for three different values of the metallicity,  $Z = 0.2Z_{\odot}$ ,  $Z_{\odot}$ , and  $2Z_{\odot}$ . We then compared the continuum spectra of the resulting models and LBDS 53W091 over the spectral range  $\lambda\lambda 2000 - 3500\text{\AA}$  (see Figure 14). Since the Kurucz model atmospheres incorporate poorly known opacities for the UV metal absorption lines and are known to poorly reproduce some of the details of the UV spectra of F (and later-type) stars, the hottest main-sequence star permissible in the composite spectrum is primarily constrained by the general shape of the spectrum and the flux at  $\sim 2200\text{\AA}$ .

The best fitting composite Solar metallicity main-sequence model has a blue limiting (i.e., “turnoff”) temperature of  $T_{\text{eff}} = 6900\text{ K}$  which corresponds to a stellar mass of  $1.35 M_{\odot}$  and a main-sequence lifetime of  $3.5\text{ Gyr}$ . The stellar ages for main-sequence stars in this mass range are robust, and are not strongly affected by uncertainties in mass loss rates, convective overshooting, mixing length theory, or the equation of state. The best fitting Solar and twice Solar metallicity main-sequence models are also able to reproduce the  $2640\text{\AA}$  break amplitude and observed  $(R - K)$  color at an age of  $\gtrsim 3.5\text{ Gyr}$ , but do not reproduce the  $2900\text{\AA}$  break or the  $(J - K)$  and  $(H - K)$  colors until ages of  $> 5\text{ Gyr}$  (see Figures 15 and 16). The  $0.2Z_{\odot}$  model is unable to reproduce the breaks or the  $(R - K)$  color for ages less than  $6\text{ Gyr}$ , and the IR colors for ages less than  $13\text{ Gyr}$ . We note here that the variation of the break amplitudes with age is very similar for the main-sequence model described here and the “full” evolutionary model (which includes the post-main sequence stars) described below in § 4.4.4; this ratifies our assumption that the breaks are dominated by starlight from the main-sequence population of stars over the relevant range of ages.

The inconsistent ages determined from fitting the rest frame UV spectrum (including the break amplitudes) versus those determined using the optical and near-IR broad-band colors most likely result from the absence of post-main-sequence stars in these models. Another possibility which we explore below is that LBDS 53W091 has a composite spectrum of two stellar populations. In populations of ages  $> 1\text{ Gyr}$ , the light at rest frame optical wavelengths (observed near-IR) contains a significant contribution from these evolved stars, and therefore the main-sequence models described here should only be applied to the rest frame UV light. With this caveat in mind, the minimum age derived from the main-sequence Solar metallicity models is  $\approx 3.5\text{ Gyr}$ .

#### 4.4. Evolutionary Models

In this section we discuss age estimates derived by fitting the spectrum of LBDS 53W091 with the evolutionary population synthesis models of Bruzual and Charlot (1997), Worthey (1994), Guiderdoni and Rocca-Volmerange (1987), and our own synthesis model (Jimenez et al. 1997). (We are indebted to Drs. Alessandro Bressan, Stephane Charlot, and Guy Worthey for their assistance in our model-fitting attempts, and in the examination of the details of the models.) The Bruzual and Charlot (1997) and the Guiderdoni and Rocca-Volmerange (1987) models incorporate only Solar metallicity libraries (from *IUE* and *OAO* in the UV). The Worthey (1994) models utilize the Kurucz (1992) theoretical stellar atmospheres as the input UV spectral library, and therefore can be used to determine spectral synthesis ages as a function of metallicity and thereby investigate the age-metallicity degeneracy. It is important to note that the Kurucz model atmospheres incorporate poorly known opacities for the UV metal absorption lines and therefore do not adequately reproduce some of the details of the UV spectra of F (and later-type) stars; hence, the age of LBDS 53W091 determined from these models is primarily constrained by the general shape of the spectrum and the flux at  $\sim 2200\text{\AA}$ . We compute all models for ‘instantaneous burst’ star formation scenarios, i.e., star formation lasting  $\lesssim 10^7$  yr. The implications of this assumption are discussed in § 5. We found that the spectral discontinuities at rest wavelengths  $\lambda 2640\text{\AA}$  and  $\lambda 2900\text{\AA}$  as well as the UV color index (defined in § 4.1) are useful discriminants between the models. In Table 4 we present the amplitudes of these indices for LBDS 53W091, some composite F and G stars, and the elliptical galaxies discussed in § 4.2. In Figure 15 we plot these breaks as a function of age for the models discussed below. In Figure 16 we plot the  $(R - K)$  color as a function of age for these same models.

As a useful control, we also analyze M32 using the same criteria and models. As discussed in the previous section, M32 has an intermediate-age stellar population ( $\sim 4$  Gyr) whose radiation should dominate in the near-UV part of the spectrum.

##### 4.4.1. Bruzual-Charlot Models

One of the most widely used evolutionary synthesis models is that of Bruzual and Charlot (1993; see also Charlot & Bruzual 1991, Bruzual 1983). In their present version (“BC95”; Bruzual and Charlot 1997), these models only incorporate evolutionary tracks and spectra for stars of Solar metallicity. These models produce very red optical-infrared colors shortly after the initial burst of star-formation: the observed optical-infrared color of LBDS 53W091 ( $R - K = 5.75$  at  $z = 1.55$ ) is reproduced at  $\approx 1.2$  Gyr (depending slightly upon the assumed IMF) after the initial burst (see Figure 16). Fitting the overall shape of the rest frame UV spectrum results in a best-fit age of 1.3 Gyr. However, to also produce the spectral discontinuities of the strengths observed in LBDS 53W091 an age in excess of 3.5 Gyr is required. Figure 15 and 16 illustrate the inconsistencies in population ages derived from these evolutionary models, if a single burst is



demanded for simplicity.

In Table 7 we see a similar quandry when BC95 is used to age-date M32. The  $R_{UV}$  color index yields an extremely young ages ( $\sim 1.3$  Gyr) for M32, and is inconsistent with the results discussed in § 4.2. The break amplitudes, however, lead to more reasonable ages of  $\gtrsim 3.5$  Gyr, suggesting that greater weight should be placed on the BC95 model fits to the spectral breaks, rather than on the fits to the overall spectrum. This procedure then suggests a large age for LBDS 53W091: the BC95 model fits to the spectral breaks imply ages of  $\sim 6$  Gyr. Accounting for the large error ranges in the break amplitude measurements for LBDS 53W091, the BC95 models suggest a minimum age of  $> 2.0$  Gyr (Figure 15).

#### 4.4.2. *Worthey Models*

Recently, models constructed by G. Worthey have been employed to age-date the populations in elliptical galaxies by using indices determined from the rest frame optical spectrum (Worthey 1994, Worthey et al. 1996). Dr. Worthey has kindly computed some UV models with metallicities of  $[\text{Fe}/\text{H}] = \pm 0.2, 0.0$  at various ages; a good fit to the UV spectrum and the  $(R - K)$  color of LBDS 53W091 occurs for the Solar metallicity models at an age of  $\sim 1.4$  Gyr (Figure 16). However, as in the case of the Bruzual and Charlot models, the breaks at 2640, 2900 Å are not reproduced at this age. For Solar abundance models, the 2640Å and 2900Å break amplitudes are only reproduced at ages of roughly 1.5 Gyr and 4.3 Gyr respectively. Allowing the metallicity to vary, we find that the break amplitudes increase more (less) rapidly for the higher (lower) abundance models. For the three metallicities considered, no models are capable of reproducing both the detailed spectroscopic features of LBDS 53W091 and the broad-band colors at the same age. In fact, these models do not produce self-consistent age estimates for M32 either and the 2640Å break amplitude implies an exceedingly low estimate ( $\sim 2.2$  Gyr) for the age of M32 when compared with the current literature discussed in § 4.2. We conclude that it is premature to extrapolate these models, which were designed for the study of features in the optical spectra of nearby galaxies, into the rest frame UV.

#### 4.4.3. *Guiderdoni & Rocca-Volmerange Models*

We also estimated the age of LBDS 53W091 using the most recent version of the evolutionary synthesis models of Guiderdoni and Rocca-Volmerange (1987, hereinafter G&RV). These models, like the BC95 models, only incorporate a Solar metallicity stellar library, and therefore cannot be used to investigate variations in metallicity. They only reproduce the rest frame UV spectrum at an age of  $\approx 4$  Gyr (see Figure 17). Satisfyingly, the infrared colors [ $R - K \approx 5.75, J - K \approx 1.75, H - K \approx 0.75$ ] are also reproduced at roughly the same age, although the break amplitudes imply an even older age ( $\approx 6.5$  Gyr). The G&RV models are therefore roughly self-consistent and

imply a large age for LBDS 53W091.

#### 4.4.4. *Jimenez Synthesis Models*

In order to have an independent check on the model-dependent age estimates (cf. Charlot et al. 1996), we constructed our own population synthesis code (Jimenez et al. 1997). The code uses interior stellar models computed using JMSTAR9 (James MacDonald, personal comm.) which incorporates the latest OPAL opacity calculations (see Iglesias & Rogers 1996 and references therein); for the low temperature atmospheres we incorporated the opacities from Alexander & Ferguson (1994) (Alexander, personal comm.). Models were computed for three values of metallicity ( $0.2Z_{\odot}$ ,  $Z_{\odot}$  and  $2Z_{\odot}$ ). Since present-day elliptical galaxies show evidence for enhancements in  $\alpha$ -process elements whereas Fe-peak elements may be under-enhanced (Worthey, Faber & Gonzalez 1992; Weiss, Peletier & Matteucci 1995), we also computed tracks for  $\alpha$ -enhanced metallicities to study the effects on the integrated spectra. In total, approximately 1000 tracks (from the contracting Hayashi track up to the TP-AGB) were computed for stars in the mass range  $0.1 M_{\odot}$  to  $120 M_{\odot}$ . These synthesis models are similar to the main-sequence models described in § 4.2, but they also incorporate the late stages of stellar evolution. We hereafter refer to these models as the ‘full’ models.

The code allows us to control the stellar physics that we input into the integrated population, and it is straightforward to investigate, for example, different mass loss laws, mixing length parameters, or Helium abundance. For the late stellar evolutionary stages (RGB, AGB and HB), we used the procedure described in Jimenez et al. (1997) to follow the evolution of stars from the base of the RGB to the TP-AGB phase. The mass loss on the RGB and AGB was approximated using the empirical parametrizations of Reimers (1975; see also Reimers 1977) and Vassiliades & Wood (1993) respectively. This procedure allows different scenarios for stellar evolution to be investigated quickly and reliably. Since the light from stars in post-main-sequence stages of stellar evolution contribute little to the total UV emission, the age determination using these models is insensitive to the exact parameters chosen to calculate the late stage evolution. We were careful not to overpopulate the post-main-sequence stages, and used the fuel consumption theorem to compute the relative number of stars in main sequence and post main-sequence phases. The set of Kurucz (1992) atmospheric models was used to compute the integrated stellar spectra of the population.

We calculated integrated spectra for populations spanning ages from 1 to 13 Gyr, and estimated the age for LBDS 53W091 using spectral fitting. The lower panel of Figure 14 shows the spectrum of LBDS 53W091 compared with synthetic spectra at three different model ages (1, 3 and 5 Gyr). An age of 2.5 Gyr (for Solar metallicity) gives a best fit to the overall spectrum and also matches the observed IR colors. The UV light in the ‘full’ models at ages  $\lesssim 4$  Gyr is almost completely dominated by the main-sequence stars. It is therefore not surprising that these ages are in good agreement with those derived from main-sequence models. The effect of using the  $\alpha$ -enhanced

tracks was to reduce the estimated age by  $\approx 0.2$  Gyr.

The model fits to the  $B(2640)$  and  $B(2900)$  break amplitudes yield ages of 3.8 and 6.6 Gyr for LBDS 53W091. The situation is similar for M32, where the fit to the UV color index gives an age of 3.7 Gyr, while  $B(2900)$  implies an age  $\sim 5.8$  Gyr. Comparing the model fits to the break amplitudes and the UV color in Tables 6 and 7, we see that Jimenez’s full models imply that LBDS 53W091 and M32 are of comparable ages.

#### 4.5. Summary of Age Estimation

In Tables 6 and 7 we compare the age estimates from our various methods. The “Mean Age” column in Table 6 lists the average of all the age estimates from a given model. The different models result in a wide range of ages for LBDS 53W091, partly due to differences in their treatments of the post–main sequence evolutionary phases (AGB, post–AGB, horizontal branch, etc; Charlot et al. 1996) as well as differing UV spectral libraries (*IUE* versus Kurucz theoretical spectra). As mentioned above, the Kurucz atmospheric models incorporate poorly known opacities for the UV metal absorption lines and inadequately reproduce the detailed UV spectra of F (and later-type) stars. Hence, the ages derived from most of the evolutionary synthesis models described above are primarily constrained by the overall shape of the UV spectrum and the spectral “bump” at  $\lambda_{rest} \sim 2200\text{\AA}$ . We therefore place the largest weight on the age determinations resulting from the newest models which incorporate the most recent opacity tables (i.e., the Jimenez “full” models) and those derived from the comparison of the break amplitudes measured in LBDS 53W091 with those measured in other objects. Finally, since the predicted  $B(2900)$  break amplitude shows much less scatter among the different models, we believe that this break provides the most reliable age–estimate; this is endorsed by the small scatter in  $B(2900)$  exhibited by the main–sequence *IUE* stars (Figure 12).

Ignoring the extrema, the model fitting as a whole suggests a minimum age of  $\approx 3.5$  Gyr for the population dominating the UV light from LBDS 53W091. The  $B(2900)$  break amplitude by itself suggests a lower limit of  $\approx 4$  Gyr; including only the Jimenez “full” models and the  $B(2900)$  break amplitude results in a lower limit of  $\approx 3.4$  Gyr. It is important to note that none of the age–estimates in Table 6 that are based on the break amplitudes are discrepant with a minimum age of  $\sim 3.5$  Gyr with the exception of those derived from the Worthey models. The ages based on the  $(R - K)$  color and the  $R_{UV}$  index are also slightly lower than those determined from the  $B(2900)$  break; this is not fully understood, and may be indicative of a mixed population (i.e., with a spread of ages; cf., González 1993), or a signature of a diluting UV component, or simply the inadequacy of the input spectral libraries. Whatever the cause, it is important to note that any correction for other components to the UV light (e.g., § 4.9) results in even stronger break amplitudes, and therefore larger ages. The minimum age of 3.5 Gyr resulting from the model fitting, is therefore a strong lower limit to the age of LBDS 53W091.

A comparison of the age–dating results for LBDS 53W091 (Table 6) with a similar analysis for M32 (Table 7) suggests that the populations dominating the UV light in these two systems have similar ages. Since the overall UV spectrum of LBDS 53W091 is slightly bluer than that of M32, it is likely that the  $z = 1.55$  galaxy is slightly younger than M32. Given the inconsistencies between the various models and the current uncertain age of the UV population in M32, we will adopt the conservative minimum age estimate of 3.5 Gyr for the remainder of this paper.

#### 4.6. The IMF and Star Formation History

The age estimates derive in the previous sections depend little on the exact form of the IMF, so long as it is smooth and the slope and the upper and lower mass cut-offs are reasonable. However, the above age estimates are all predicated on the absence of young, hot (i.e., O, B, and A) stars in the spectrum of LBDS 53W091. The possibility therefore exists that the spectrum of LBDS 53W091 merely reflects an IMF devoid of high mass stars and that the galaxy is young. No direct evidence exists that the galaxy contains evolved giants. However, a truncated IMF would be a rather contrived explanation for LBDS 53W091’s spectrum, requiring an IMF that cut off exactly at spectral type F6V to escape the above age estimates. With no stars  $\gtrsim 1.5 M_{\odot}$ , the genesis and disbursement of metals within the galaxy becomes problematic, though the effect of these constituents are clearly visible in the Mg II 2800 absorption line as well as the spectral breaks at 2640Å and 2900Å. Furthermore, discussions of truncated IMFs usually involve a suppression of the *low* mass stars to escape the G–dwarf problem (e.g., Charlot et al. 1993). Starbursts appear to favor high–mass stars. We therefore find truncating the IMF a contrived explanation for LBDS 53W091’s spectrum.

The derived age estimates are also predicated on the assumption of an instantaneous burst of star formation. The implications of this conservative assumption are discussed in § 5, though the possibility exists that the UV spectrum of LBDS 53W091 reflects multiple bursts of star formation. In the particular case of double–burst star formation scenarios, the UV continuum and UV color are dominated by the youngest stars while the break amplitudes reflect the older stars diluted by the flatter spectrum younger population. For example, using the BC95 models, the UV continuum slope of LBDS 53W091 is reproduced shortly after each burst, but at these young ages the model breaks are always overly suppressed by the hot stars, implying that no simple double–burst scenario can satisfactorily fit all criteria simultaneously. This is perhaps unsurprising when one considers the ages derived for M32 in Table 7: it is *highly* unlikely that M32 has a stellar population younger than 2 Gyr, implying that the low ages derived from the UV continuum spectra are more emblematic of the weaknesses of the current generation of UV evolutionary models rather than a complicated star formation history.

#### 4.7. Age-Metallicity Degeneracy

As is clear from the spectral synthesis models described in § 4.3 and 4.4, more metal rich populations can reproduce the rest frame UV spectrum of LBDS 53W091 at younger ages. Metal poor populations with metallicities of  $0.2Z_{\odot}$ , on the other hand, can only reproduce the shape of the UV spectrum and the break amplitudes at ages greater than 5 Gyr. This is the well-studied problem of the age-metallicity degeneracy that plagues population synthesis; in the case of the nearby elliptical galaxies, several optical spectral indices (involving hydrogen and metal lines) have been devised to separate the effects of age and metallicity (e.g., Worthey 1994, Gorgas et al. 1993, Jones 1996).

Unfortunately, the optical faintness of LBDS 53W091 ( $R \approx 24.5$ ) precludes a direct measurement of the metallicity, especially because the hydrogen Balmer and metal line indices commonly used to break the age-metallicity degeneracy are redshifted into the near-IR for redshifts  $z > 1.2$ . It is possible that future efforts with infrared spectrographs and adaptive optics on large telescopes will permit a measurement of abundances in the integrated light using features that are well-studied in local elliptical galaxies. For the present, the age estimates of LBDS 53W091 remain degenerate with metallicity.

However, if we assume that LBDS 53W091 is a progenitor of a present-day elliptical galaxy and that no active star formation has taken place over the last  $\sim 11$  Gyr (lookback time to  $z = 1.55$  for  $H_0=50$ ,  $\Omega_0 = 0.2$ ), then the mean metallicity of LBDS 53W091 should be very similar to that found for local  $\gtrsim L^*$  elliptical galaxies. Nearby elliptical galaxies with luminosities larger than  $L^*$  generally have spatially integrated metallicities (determined from the integrated spectrum) that are approximately Solar (Worthey et al. 1984; Kormendy & Djorgovski 1989; Worthey, Faber & González 1992; Sadler 1992). Within the effective radius  $R_e$ , the luminosity-averaged metallicity of nearby luminous ellipticals is roughly Solar. For example, the Mg index of luminous ellipticals is  $\approx 0.30$  in the nuclear regions (i.e., super-Solar metallicity of  $[\text{Mg}/\text{H}] = +0.2$  in the core), whereas it decreases to  $\approx 0.22$  at radii near  $R_e$  (Buzzoni 1996), implying sub-Solar metallicities,  $[\text{Mg}/\text{H}] \sim -0.3$  to  $-0.4$ . Gonzalez & Gorgas (1996) present Mg index profiles for several giant ellipticals, again suggesting a similar mean Mg index of  $\sim 0.22$  for radii of  $0.5 R_e$  to  $R_e$ . Arimoto (1996) concludes that a mean metallicity of Solar is appropriate for nearby ellipticals based on measurements of the abundance in the hot corona and old stars.

The effective radius,  $R_e$ , of an  $L^*$  galaxy at  $z = 1.55$  is  $\approx 0''.7$  (e.g., Dickinson 1995). Hence, our  $1''$  spectroscopic slit samples the galaxian profile to almost  $R_e$ . It is therefore reasonable to assume that the UV population in LBDS 53W091 has a metallicity which is approximately Solar within the aperture of our observations. Even for twice Solar metallicity, the break amplitudes imply an age in excess of 3 Gyr for LBDS 53W091 (see Dunlop et al. 1996, Figure 2c).

#### 4.8. Dust Reddening and the Age Limit

Thus far, we have avoided the conclusion that dust reddening of a young stellar population is responsible for the red color of LBDS 53W091. The most important objection to strong dust reddening is that stellar populations younger than  $\approx 2-3$  Gyr fail to reproduce the spectral features observed in the rest frame UV spectrum. In addition, the  $B(2640)$  and  $B(2900)$  spectral breaks used in the preceding discussion are defined over short, adjacent wavelength intervals of the UV spectrum, and are therefore virtually reddening independent. We noted earlier that in most cases, the  $B(2640)$  and  $B(2900)$  continuum breaks suggested an age similar to that implied by the broader baseline  $R_{UV}$  color index, suggesting that the reddening is negligible. As a test, we dereddened the spectrum using an LMC extinction law and an  $E(B - V) = 0.1$  (i.e.,  $A_B \approx 0.4$ ). The best fitting Bruzual and Charlot model to this dereddened spectrum has an age of  $\approx 1.3$  Gyr but provides a poor fit to the break amplitudes and the optical-IR colors.

For the remainder of this paper we consider 3.5 Gyr a minimum for galaxy LBDS 53W091. A similar minimum age is likely to apply to galaxy 3a, by virtue of its spatial proximity to LBDS 53W091 and its similar spectral energy distribution. The implications of finding two very red galaxies in close proximity and at similar redshifts is discussed in § 5.

#### 4.9. Other Contributions to the UV Light

##### 4.9.1. Active Galactic Nucleus

The AGN may contribute to the ultraviolet continuum emission in LBDS 53W091, either directly or by dust and electron scattering as it typically does in more powerful radio galaxies (e.g., di Serego Alighieri et al. 1989; Cimatti et al. 1993; Jannuzi et al. 1996; Dey & Spinrad 1996). The AGN continuum would tend to dilute the spectral features and the break amplitudes, and hence accounting for this component in the spectrum would make the intrinsic break amplitudes even larger and imply an even older age. Since the breaks at 2640Å and 2900Å are already strong, are comparable to those in individual stars, and fail to be reproduced by most of the population synthesis models, it is unlikely that the AGN contribution is significant at UV wavelengths. A second indication that the AGN contribution is likely to be very minimal is the apparent lack of strong emission lines in the UV spectrum: the limits on the C II], C III] and Mg II emission lines are roughly 10 times fainter than that observed in powerful (3CR) radio galaxies at similar redshifts (McCarthy 1993).

We can make a rough estimate of the UV contribution from an AGN in LBDS 53W091 by comparing it with the powerful 3CR radio galaxies. The radio power at 1.4 GHz of LBDS 53W091 is approximately 50 times smaller than that of a typical 3CR radio galaxy at  $z \gtrsim 1.5$ . If the UV luminosity of the AGN is also reduced by this factor, the observed  $R$  band magnitude (rest frame  $\sim 2700$  Å) of LBDS 53W091 would be  $\approx 26$  mag, or approximately one third of the observed

near-UV flux. This contribution, if present, would only dilute the break amplitudes, implying an even greater age for LBDS 53W091. Since the present age estimate already provides stringent constraints to the cosmological parameters, it is unlikely that the diluting AGN contribution is significant.

#### 4.9.2. Blue Stragglers

In old Galactic star clusters, blue stragglers (thought to be hot binary stars or stellar merger remnants) can contribute significantly to the total short wavelength UV flux from the cluster. These stars are brighter, and often considerably bluer than the stars near the main-sequence turnoff in cluster color-magnitude diagrams. Most importantly, they are not represented in any of the contemporary theoretical isochrones used by extant spectral synthesis models. Thus, if the integrated spectra of galaxies are similar to those of old Galactic clusters and contain a contribution from a blue straggler population, the present synthesis models will underestimate their age.

To examine the situation quantitatively, we utilized color-magnitude arrays (Milone & Latham 1994) and a luminosity function from M67 (Montgomery et al. 1993, Fan et al. 1996) for the clusters listed in Table 8. We crudely estimated the blue straggler contribution to the integrated UV light from clusters ( $\lambda_{\text{rest}} \sim 2600\text{\AA}$ ) under the assumption that the blue stragglers have UV spectra resembling their main-sequence ( $B - V$ ) analogs and assuming that the mass function determined for M67 (Montgomery et al. 1993) is applicable to all clusters. For M67 itself, our most robust blue straggler case, these stars contribute approximately one half of the total light at  $2600\text{\AA}$ . At the other extreme, the solitary bright blue straggler star in NGC 752 makes up only 20% of the integrated UV flux from the cluster. The other clusters listed in Table 8 lie roughly between these extremes.

Hence, if the stellar content of LBDS 53W091 is similar to that of the Galactic clusters, blue stragglers *may* be responsible for as much as  $\sim 20\% - 50\%$  of the UV flux. Accounting for this contribution will, as in the case of the AGN, increase the age of the turnoff population. Our reliance on the isochrone models described in § 4.3 for estimating the age of LBDS 53W091 spectrum is undoubtedly naive; however, most of the substantive uncertainties point toward our mean age of 3.5 Gyr (or *any* age determined using these models) being a lower bound.

## 5. On the Formation History of LBDS 53W091 and Cosmological Implications

The 3.5 Gyr minimum age we deduce in § 4 is almost certainly a significant under-estimate of the true age of LBDS 53W091. First, this age assumes that the fairly large elliptical galaxy was formed in an instantaneous stellar burst after which star formation completely ceased. More realistically, the initial episode of star formation is likely to last at least one dynamical collapse time,  $\gtrsim 2 \times 10^8$  yrs. If one assumes an extended episode of star formation, the derived total age

increases in direct agreement with the assumed duration of the star formation burst; the ages derived in § 4 are actually the time elapsed since the cessation of star formation in the galaxy, since the UV spectrum for old populations is dominated by stars at the main–sequence turnoff. Second, it is rather unlikely that the turnoff population that dominates the UV starlight is a result of the *first* episode of star formation. Because the metallicity of the population is almost certainly non-primordial, the gas from which the present UV–dominant population was formed must have been enriched by previous episodes of star formation. The duration of these previous star forming episodes, and the time between the earlier episodes and the present one, must also be added to the age of the galaxy. Future spectroscopic observations of LBDS 53W091 in the near– and mid–IR may allow us to determine its giant content and thereby constrain the contribution from previous bursts to the integrated spectrum. Therefore, in accounting for the original dynamical collapse time of the galaxy, and multiple, non–instantaneous episodes of star formation, the adopted ‘age’ of 3.5 Gyr is found to provide a conservative lower bound to the true age of the galaxy.

Independent of cosmology, the discovery of a high redshift galaxy with a spectrum nearly identical to that of nearby, old elliptical galaxies has the profound implication that the epoch of formation of these early type systems must be at very high redshifts ( $z \geq 5$ ). If the other red galaxies which lie nearby (in projection) are indeed physically associated with LBDS 53W091, they raise the additional problem of an early epoch for structure formation.

An old galaxy at  $z = 1.552$  can impose strong constraints on the time–scale for cosmology, the epoch of the last burst of star–formation and, perhaps, the epoch of galaxy assembly. We consider first cosmologies without a cosmological constant ( $\Lambda = 0$ ). Figure 18a shows the parameter space of the  $H_0 - \Omega_0$  plane allowed by the existence of a 3.5 Gyr old galaxy at a redshift  $z = 1.552$  (the hatched region is excluded). Recent measurements of  $H_0$  (Kennicutt et al. 1995; Sandage et al. 1996) imply values between 50 and 80  $\text{km s}^{-1} \text{Mpc}^{-1}$ . Figure 18 simply re–illustrates the familiar time–scale problem resulting in studies of the ages of Galactic globular clusters. In the present case, the age problem is referred to a time when the Universe was less than 30% of its present age, and the uncertainties are largely independent of those encountered in the globular cluster studies. The existence of LBDS 53W091 permits only low Hubble constants and/or low cosmic densities; in particular, an  $\Omega = 1$  Universe requires  $H_0 \lesssim 45 \text{ km s}^{-1} \text{Mpc}^{-1}$ . With  $H_0 = 50 \text{ km s}^{-1} \text{Mpc}^{-1}$ , a Universe with  $\Omega_0 \lesssim 0.2$  is acceptable; for this cosmology we derive a formation redshift for LBDS 53W091 age of  $z_f \geq 5$ .

A possible solution to the age paradox is to invoke a non–zero cosmological constant. Figure 18b illustrates the constraints on the  $H_0 - \Omega_\Lambda$  parameter space for a flat ( $\Omega_{\text{total}} = \Omega_0 + \Omega_\Lambda = 1$ ) universe imposed by a 3.5 Gyr old galaxy at a redshift of  $z = 1.552$ . *HST* counts of ellipticals down to  $I \approx 24.5$  ( $B \approx 26.5$ ) imply  $\Omega_\Lambda \leq 0.8$ , with a likely range of  $\Omega_\Lambda \lesssim 0.5$  (Driver et al. 1996). *COBE* measurements of the cosmic microwave background imply a similar upper limit,  $\Omega_\Lambda \leq 0.5$  for  $H_0 = 70 \text{ km s}^{-1} \text{Mpc}^{-1}$  (White & Bunn 1995), as do analyses of gravitational lens statistics ( $\Omega_\Lambda < 0.66$  at the 95% confidence level, Kochanek 1996) and high–redshift supernovae ( $\Omega_\Lambda < 0.51$  at the 95 % confidence level, Perlmutter et al. 1996). LBDS 53W091 implies a *lower* limit to  $\Omega_\Lambda$



(for  $\Omega_{\text{total}} = 1$ ): for  $H_0 > 50 \text{ km s}^{-1} \text{ Mpc}^{-1}$ , we find  $\Omega_{\Lambda} \gtrsim 0.15$ , while for  $H_0 > 70 \text{ km s}^{-1} \text{ Mpc}^{-1}$ ,  $\Omega_{\Lambda} \gtrsim 0.5$ . For certain values of the cosmological parameters, LBDS 53W091 thus provides tighter (and independent) constraints than the well-known globular cluster age limits.

If the old, red, and “dead” elliptical galaxies that we now observe at intermediate redshifts ( $z \lesssim 1$ ) really did form this early, and if their initial starburst phase had a short duration, some luminous galaxies near  $z = 6$  should eventually be observable in the near-IR domain, and should be identifiable by their Lyman limit cutoff in the optical part of the spectrum. If, however, the typical formation redshift is much larger (e.g.,  $z_f \geq 10$ ), these elusive objects await discovery by NICMOS on the *HST*.

## 6. Conclusions

We have observed the weak radio source LBDS 53W091, associated with a very faint red galaxy ( $R \approx 24.5$ ,  $R - K \approx 5.8$ ). Deep exposures with the W.M. Keck telescope reveal a spectrum devoid of strong emission lines, and dominated by starlight from a red stellar population. Based on the 2640Å and 2900Å spectral breaks, we determine the absorption line redshift of the galaxy to be  $z = 1.552 \pm 0.002$ . The rest-frame UV spectrum, generally dominated by the main-sequence turnoff population in intermediate-age coeval populations, is similar to that of late F stars. The best-fit turnoff spectral type of F6V suggests a strict lower limit of  $\sim 2.5$  Gyr for the age of LBDS 53W091, implying that it is the oldest galaxy yet discovered at  $z \gtrsim 1$ . It is important to note that the amplitudes of the UV continuum spectral breaks at 2640Å and 2900Å, as well as the broader baseline UV color index are all consistent with a main sequence turnoff color of  $(B - V) \approx 0.5$  (i.e., a spectral type of F6V). Since the UV color index is more easily affected by dust than the spectral breaks, the consistent turnoff color estimates strongly suggest that the dust reddening in LBDS 53W091 is minimal. The rest-frame UV spectrum of LBDS 53W091 is very similar to (albeit slightly bluer) than that of the well-studied nearby ellipticals M32 and NGC 3610. Since the UV light in these nearby systems is dominated by an intermediate-age stellar population ( $\sim 4$ –5 Gyr) in addition to the old population typical of ellipticals, the population dominating the UV light in LBDS 53W091 is likely to be of comparable age.

We have also estimated the age of LBDS 53W091 (i.e., the time elapsed since the last major epoch of star formation) using a variety of spectral synthesis models. Using the synthesized spectra of composite *main-sequence* stellar populations of varying metallicity, we find a best fit age of 3.5 Gyr for Solar metallicity. We also fit the spectrum using the current evolutionary population synthesis models of Bruzual and Charlot (1997), Jimenez et al. (1997), Worthey (1994), and Guiderdoni and Rocca-Volmerange (1987). We find that the different models do not result in self-consistent ages for either LBDS 53W091 or the nearby, well-studied elliptical M32. These inconsistencies are likely due to differing treatments of stars in their evolved stages, as well their reliance on differing UV stellar spectral libraries and the uncertainties in the metallicities. The most robust self-consistent age estimates result from model (and single star) fits to the 2900Å

break amplitude, and from the models which incorporate the newest opacity tables. We conservatively combine the various age estimates and derive a *minimum* age of 3.5 Gyr for LBDS 53W091. Finding such an old galaxy at these large lookback times has important cosmological consequences. In particular, this result effectively rules out  $H_0 \gtrsim 45 \text{ km s}^{-1} \text{ Mpc}^{-1}$  for  $\Omega = 1$ .

We are grateful to Mark Dickinson, Wayne Wack, Terry Stickel, Randy Campbell and Tom Bida for their invaluable help on our Keck observing runs. We are also very grateful to Alessandro Bressan, Stephane Charlot, Ben Dorman and Guy Worthey for their generous help and advice on the various stellar spectral synthesis models presented in this paper. We thank Yong Li and Dave Burstein for providing us with the digitized version of the *IUE* stellar spectral atlas, and Dave Burstein, Harry Ferguson, and Mike Eracleous for providing us with the UV spectra of M32 and NGC 3610. We thank John Davies for carrying out the UKIRT service observations, Dave Silva for useful discussions regarding nearby ellipticals and Ata Sarajedini for providing us with the most recent version of the Revised Yale Isochrones. Finally, we thank the referee Jim Schombert for an extremely prompt and useful referee report. The W. M. Keck Telescope is a scientific partnership between the University of California and the California Institute of Technology, made possible by a generous gift of the W. M. Keck Foundation. The United Kingdom Infrared Telescope is operated by the Royal Observatories on behalf of the UK Particle Physics and Astronomy Research Council. The National Optical Astronomy Observatories are operated by the Association of Universities for Research in Astronomy under Cooperative Agreement with the National Science Foundation. This work was supported by the US National Science Foundation (grant # AST-9225133 to HS and AST-8821016 to RAW), by an Alfred P. Sloan Fellowship to RAW and an EC Fellowship to RJ.

## REFERENCES

- Alexander, D. R. & Ferguson, J. W. 1994, ApJ, 437, 839  
Begelman, M. C. & Cioffi, D. F. 1989, ApJ, 345, 21  
Baum, W. A. 1959, PASP, 71, 106  
Bressan, A., Chiosi, C., & Fagotto, F. 1994, ApJS, 94, 63  
Bruzual A., G. 1983, ApJ, 273, 105  
Bruzual A., G. & Charlot, S. 1993, ApJ, 405, 538  
Bruzual A., G. & Charlot, S. 1997, in preparation  
Burstein, D., Faber, S. M., Gaskell, C. M. & Krumm, N. 1984, ApJ, 287, 586  
Burstein, D., Bertola, F., Buson, L.M., Faber, S.M., & Lauer, T.R. 1988, ApJ, 328, 440  
Chambers, K. C. & Charlot, S. 1990, ApJ, 348, L1  
Chambers, K. C. & McCarthy, P. J. 1990, ApJ, 354, L9

- Chambers, K. C., Miley, G. K. & van Breugel, W. 1987, *Nature*, 329, 604.
- Charlot, S. & Bruzual A., G. 1991, *ApJ*, 367, 126
- Charlot, S., Ferrari, F., Mathews, G. J. & Silk, J. 1993, *ApJ*, 419, L57
- Charlot, S., Worthey, G., & Bressan, A. 1996, *ApJ*, 457, 625
- Couch, W. J., Ellis, R. S., Sharples, R. M. & Smail, I. 1994, *ApJ*, 430, 121
- Cowie, L.L., Hu, E.M., & Songaila, A. 1995, *Nature*, 377, 603
- Cimatti, A., Dey, A., van Breugel, W., Antonucci, R., & Spinrad, H. 1996, *ApJ*, 465, 145
- Dey, A. & Spinrad, H. 1996, *ApJ*, 459, 133
- Dey, A., Cimatti, A., van Breugel, W., Antonucci, R., & Spinrad, H. 1996, *ApJ*, 465, 157
- Dey, A., Spinrad, H., Stern, D., Dunlop, J., Peacock, J., Jimenez, R., & Windhorst, R. 1997, in preparation
- De Young, D. 1981, *Nature*, 293, 43
- De Young, D. 1989, *ApJ*, 342, L59
- Dickinson, M. 1996, in *Fresh Views of Elliptical Galaxies*, ed. Buzzoni, Renzini, & Serrano (ASP Conf. Ser., 86), 283
- Dickinson, M. et al. 1997, in preparation
- Dinescu, D., Girard, T., van Altena, W., Yang, T., & Lee, Y. 1996, *AJ*, 111, 1205
- di Serego Alighieri, S., Fosbury, R.A.E., Quinn, P.J., & Tadhunter, C.N. 1989, *Nature*, 341, 307
- di Serego Alighieri, S., Cimatti, A. & Fosbury, R. A. E. 1994, *ApJ*, 431, 123
- Dressler, A., Oemler, A., Butcher, H. R. & Gunn, J. E. 1994, *ApJ*, 430, 107
- Driver, S.P., Windhorst, R.A., Ostrander, E.J., Keel, W.C., Griffiths, R.E., & Ratnatunga, K.U. 1995a, *ApJ*, 449, L23
- Driver, S.P., Windhorst, R.A., & Griffiths, R.E. 1995b, *ApJ*, 453, 48
- Driver, S.P., Windhorst, R.A., Phillipps, S., & Bristow, P.D. 1996, *ApJ*, 461, 525
- Dunlop, J. S., Peacock, J. A., Savage, A., Lilly, S. J., Heasley, J. N., & Simon, A. J. B. 1989a, *MNRAS*, 238, 1171
- Dunlop, J.S., Guiderdoni, B., Rocca-Volmerange, B., Peacock, J.A., & Longair, M.S. 1989b, *MNRAS*, 240, 257
- Dunlop, J. S. & Peacock, J. A. 1993, *MNRAS*, 263, 936
- Dunlop, J. S., Peacock, J. A., & Windhorst, R. A. 1995, in *Galaxies in the Young Universe*, ed. Hippelein, H. & Meisenheimer, K. (Proc. Ringberg Conf, Sept. 1994), in press
- Dunlop, J. S., Peacock, J. A., Spinrad, H., Dey, A., Jimenez, R., Stern, D. & Windhorst, R. A. 1996, *Nature*, 381, 581

- Eales, S. A. & Rawlings, S. 1993, ApJ, 411, 67
- Eales, S. A., Rawlings, S., Dickinson, M., Spinrad, H., Hill, G. J. & Lacy, M. 1993, ApJ, 409, 578.
- Elston & Silva, D. 1992, AJ, 104, 1360
- Fanaroff, B. L. & Riley, J. M. 1974, MNRAS, 167, 31P
- Fan, X. et al. 1996, ApJ, 112, 628
- Fanelli, M. N., O’Connell, R. W., Burstein, D. & Wu, C.-C. 1992, ApJS, 82, 197
- Freedman, W. 1992, in The Stellar Populations of Galaxies, ed. Barbury, B. & Renzini, A. (I.A.U. Symp., 149), 169
- González, J. 1993, Ph.D. Thesis, University of California at Santa Cruz
- Gorgas et al. 1993, ApJS, 86, 153.
- Green, E. M., Demarque, P. & King, C. R. 1987, “The Revised Yale Isochrones and Luminosity Functions” (Yale University Observatory, New Haven)
- Grillmair, C. J. et al. 1996, AJ, 112, 1975
- Guiderdoni, B. & Rocca-Volmerange, B. 1987, A&A, 186, 1
- Iglesias, C. W. & Rogers, F. J. 1996, ApJ, 464, 855
- Jannuzi, B. T. & Elston, R. 1991, ApJ, 366, L69.
- Jannuzi, B. T., Elston, R., Schmidt, G. D., Smith, P. S. & Stockman, H. S. 1995, ApJ, 454, L111.
- Jimenez, R. et al. 1997, in preparation
- Jones, L.A. 1996, in Fresh Views of Elliptical Galaxies, ed. Buzzoni, Renzini, & Serrano (ASP Conf. Ser., 86), 207
- Kennicutt, R., Freedman, W., & Mould, J. 1995, AJ, 110, 1476
- Kent, S. M. 1985, PASP, 97, 165
- Kochanek, C. S. 1996, ApJ, 466, 638
- Kormendy, J. & Djorgovski, S. 1989, ARA&A, 27, 235
- Kron, R. G., Koo, D. C., & Windhorst, R. A. 1985, A&A, 146, 38
- Kurucz, R. 1992, CDROM, 13
- Lacy, M. et al. 1995, MNRAS, 271, 504
- Landolt, A. U. 1992, AJ, 104, 340
- Lilly, S. J. 1989, ApJ, 340, 77
- Lilly, S. J. & Longair, M. S. 1984, MNRAS, 211, 833
- Lilly, S. J., Tresse, L., Hammer, F., Crampton, D. & Le Fèvre, O. 1995, 455, 108
- Miller, G. E. and Scalo, J. M. 1979, ApJS, 41, 513

- McCarthy, P. 1993, *ARA&A*, 31, 639
- McCarthy, P., van Breugel, W., Spinrad, H., & Djorgovski, S. 1987, *ApJ*, 321, L29
- McCarthy, P. J., Kapahi, V. K., van Breugel, W., Persson, S. E., Athreya, R. & Subramhanya, C. R. 1996, *ApJS*, in press.
- Milone & Latham 1994, *AJ*, 108, 1828
- Montgomery et al. 1993, *AJ*, 106, 181
- Morton, D.C., Spinrad, H., Bruzual, G.A., & Kurucz, R.L. 1977, *ApJ*, 212, 438
- Neuschaefter, L. W., Windhorst, R. A., & Dressler, A. 1991, *ApJ*, 382, 32
- Neuschaefter, L. W., & Windhorst, R. A. 1995, *ApJ*, 439, 1 (NW95a)
- Neuschaefter, L. W., & Windhorst, R. A. 1995, *ApJS*, 96, 371 (NW95b)
- O’Connell, R. W. 1980, *ApJ*, 236, 430
- Oke, J.B. et al. 1995, *PASP*, 107, 375
- Oke, J. B., Gunn, J. E. & Hoessel, J. G. 1996, *AJ*, 111, 29
- Oort, M. J. A., Katgert, P., Steeman, F. W. M., & Windhorst, R. A. 1987, *A&A*, 179, 41
- Oort, M. J. A., & Langevelde, H. J. 1987, *A&AS*, 71, 250
- Perlmutter, S. et al. 1996, *astro-ph/9608192*
- Rakos, K. D. & Schombert, J. M. 1995, *ApJ*, 439, 47
- Rawlings, S. & Saunders, R. 1991, *Nature*, 349, 138
- Rawlings, S., Lacy, M., Blundell, K. M., Eales, S. A., Bunker, A. J., & Garrington, S. T. 1996, *Nature*, 383, 502
- Reimers, D. 1977, *A&A*, 61, 217
- Reimers, D. 1975, *Mem. Soc. Roy. Sci. Liège*, 8, 369
- Rix & White 1992, *MNRAS*, 254, 389
- Rocca-Volmerange, B. & Guiderdoni, B. 1987, *A&A*, 175, 15
- Sadler, E. 1992, in *The Stellar Populations of Galaxies*, ed. Barbuy, B. & Renzini, A. (I.A.U. Symp., 149), 41
- Sandage, A., Saha, A., Tammann, G. A., Labhardt, L., Panagia, N., & Macchetto, F. D. 1996, *ApJ*, 460, L15
- Scalo, J.M. 1986, *Fund Cosm Phys*, 11, 1
- Schade, D. et al. 1995, *ApJ*, 451, L1
- Scorza & Bender 1990, *A&A*, 235, 49
- Silva, D. 1995, in *Spiral Galaxies in the Near-IR*, ed. Minniti & Rix (Proc. ESO/MPA Workshop, June 1995)

- Silva, D. & Bothun, G. 1997, preprint
- Spinrad, H. & Djorgovski, S. 1987, in *Observational Cosmology*, ed. Hewitt, Burbidge, & Fang (IAU Symp 124), 129
- Spinrad, H., Dey, A., & Graham, J. R. 1995, *ApJ*, 438, L51
- Stanford, S. A., Eisenhardt, P. R. M., Dickinson, M. 1995, *ApJ*, 450, 512
- Stanford, S. A., Elston, R., Eisenhardt, P., Dey, A., Stern, D., & Spinrad, H. 1997, in preparation
- Steidel, C. C., Giavalisco, M., Pettini, M., Dickinson, M. & Adelberger, K. 1996, *ApJ*, 462, 17
- Stern, D., Dey, A., Spinrad, H., Dickinson, M., Schlegel, D., & Gonzalez, R. 1997, in preparation
- Stockton, A., Kellogg, M., & Ridgway, S.E. 1995, *ApJ*, 443, L69
- Tadhunter, C. N., Morganti, R., di Serego Alighieri, S., Fosbury, R. A. E. & Danziger, J. 1993, *MNRAS*, 263, 999.
- Thuan, T. X., & Gunn, J. E. 1976, *PASP*, 88, 543
- Vassiliadis, E. & Wood, P. R. 1993, *ApJ*, 413, 641
- Vigotti, M. et al. 1996, in preparation
- Weiss, A., Peletier, R. F. & Matteucci, F. 1995, *A&A*, 296, 73
- West, M. J. 1991, *ApJ*, 379, 19
- White, M. & Bunn, T. 1995, *ApJ*, 450, 477
- Windhorst, R. A., van Heerde, G. M., & Katgert, P. 1984a, *A&A*, 58, 1 (WHK)
- Windhorst, R. A., Kron, R. G., & Koo, D. C. 1984b, *A&AS*, 58, 38 (WKK)
- Windhorst, R. A., Miley, G. K., Owen, F. N., Kron, R. G., & Koo, D. C. 1985, *ApJ*, 289, 494
- Windhorst, R.A. et al. 1991, *ApJ*, 380, 362
- Windhorst, R. A., Fomalont, E. B., Kellermann, K. I., Partridge, R. B., Richards, E., Franklin, B. E., Pascarella, S. M., & Griffiths, R. E. 1995, *Nature*, 375, 471
- Worthey, G. 1994, *ApJS*, 95, 107
- Worthey, G., Faber, S., & González, J. 1992, *ApJ*, 398, 69
- Worthey, G., Trager, S., & Faber, S.M. 1996, in *Fresh Views of Elliptical Galaxies*, ed. Buzzoni, Renzini, & Serrano (ASP Conf. Ser., 86), 203
- Wu, C. et al. 1991, IUE NASA Newsletter No. 43

Fig. 1.— VLA A-Array 4.86 GHz map of the radio source LBDS 53W091. The noise in the map is  $\sigma = 52\mu\text{Jy}/\text{beam}$ , and the contours shown are drawn at  $(-3,3,6,12,18,24,36)\sigma$ .

Fig. 2.— Keck  $R$ -band of the field of LBDS 53W091. The frame is  $1'$  on a side; north is to the top and east is to the left. The scale bar shown at top left corresponds to  $\approx 55.7$  kpc at  $z = 1.552$ . The optical counterpart of the radio source is at  $\alpha_{1950} = 17^{\text{h}}21^{\text{m}}17^{\text{s}}.78$ ,  $\delta_{1950} = 50^{\circ}08'47''.3$ , and the offset from galaxy C to LBDS 53W091 is  $\Delta\alpha = 20''.5$  (east),  $\Delta\delta = -2''.8$  (south).

Fig. 3.— (a) Detail of the Keck  $R$ -band image of LBDS 53W091. (b) Sum of the UKIRT  $J$  and  $H$  band images. Both frames are  $19''$  on a side, and north is to the top and east is to the left. The host galaxy of the radio source is labelled 53W091. The blue objects 1 and 3b are foreground emission line galaxies. Object 3a and 4 have similar optical–IR colors to LBDS 53W091 and are likely to be at the same redshift.

Fig. 4.— False color image of the field of LBDS 53W091 constructed using the images in the  $R$ -band (blue),  $J$ -band (green), and  $H$ -band (red) of the field of LBDS 53W091. Note that the host galaxy of the radio source and the two objects nearest it have roughly the same color, and may be all at a common redshift.

Fig. 5.— The 5.5 hour Keck LRIS spectrum of the host galaxy of LBDS 53W091 plotted in the observers’ frame. The upper panel shows the coadded spectrum smoothed using a boxcar filter of width 9 pixels. The lower panel shows the formal  $1\sigma$  error bars on the spectrum (averaged in 10-pixel bins). The rest wavelength is indicated along the upper abscissa for a redshift of  $z = 1.552$ . The long wavelengths suffer increased noise from atmospheric OH emission lines. The spectrum has been corrected for telluric  $\text{O}_2$  absorption in the A- and B-bands.

Fig. 6.— Spectra of LBDS 53W091 (shifted) and galaxy 3a plotted in the observers’ frame. The spectra have been averaged in 25-pixel bins. The rest wavelength is indicated along the upper abscissa for a redshift of  $z = 1.552$ . The  $2900\text{\AA}$  discontinuity apparent in both objects. We interpret galaxy 3a to be a faint companion to LBDS 53W091 with both similar age and redshift.

Fig. 7.— Spectra of the blue emission line galaxies labelled “1” (upper panel) and “3b” (lower panel) in Figure 3. The spectra are plotted in the observed frame. The parameters of the emission lines are listed in Table 3.

Fig. 8.— Rest frame spectrum of LBDS 53W091 plotted against scaled averages of  $IUE$  stars. Note that the spectrum of the average F6V stellar type the galaxy spectrum almost perfectly. Assuming Solar metallicity Revised Yale Isochrones, this implies a minimum age just less than 3 Gyr for the bluest turn-off.

Fig. 9.— Rest frame spectra of LBDS 53W091 (Keck), M32 ( $IUE$ ; Burstein et al. 1988), and NGC 3610 ( $HST$ ; Ferguson, private communication), where the latter two galaxy spectra have been scaled and offset. Note the similarity in the spectral features. NGC 3610 is a moderately

Table 1. Radio Data<sup>†</sup>

Component	$RA_{1950}$	$DEC_{1950}$	$\nu$ (GHz)	$F_\nu$ (mJy)
Total	$17^h21^m17^s81 \pm 0^s01$	$+50^\circ08'47''6 \pm 0''1$	1.565	$23.0 \pm 1.7$
			4.860	$6.5 \pm 0.4$
SE Lobe	$17^h21^m17^s98 \pm 0^s01$	$+50^\circ08'46''18 \pm 0''05$	1.565	$11.5 \pm 1.3$
			4.860	$3.37 \pm 0.23$
NW Lobe	$17^h21^m17^s64 \pm 0^s01$	$+50^\circ08'49''00 \pm 0''07$	1.565	$10.7 \pm 1.3$
			4.860	$2.25 \pm 0.29$

<sup>†</sup>Data in this table are derived from the 1995 VLA observations described in the text.

Table 2. Photometry in the LBDS 53W091 Field.

	Galaxy 1	LBDS 53W091	Galaxy 3a	Galaxy 3b	Galaxy 4
<i>R</i>	$23.9 \pm 0.1$	$24.5 \pm 0.2$	$24.9 \pm 0.2$	$25.1 \pm 0.3$	$25.5 \pm 0.3$
<i>J</i>	$22.1 \pm 0.5$	$20.5 \pm 0.1$	$20.5 \pm 0.1$	$22.2 \pm 0.5$	$20.6 \pm 0.2$
<i>H</i>	$21.5 \pm 0.4$	$19.5 \pm 0.1$	$19.5 \pm 0.1$	$21.5 \pm 0.4$	$20.0 \pm 0.1$
<i>K</i>	$19.8 \pm 0.3$	$18.7 \pm 0.1$	$18.9 \pm 0.2$	$20.1 \pm 0.5$	$19.0 \pm 0.3$

Note. — All magnitudes are measured in a  $4''$  diameter aperture.



Table 3. Line Identifications in the Blue Galaxies.

Source	$\lambda_{\text{obs}}$ Å	Line ID	Flux ( $10^{-17}$ erg cm $^{-2}$ s $^{-1}$ )	$z$
Galaxy 1	5897:	Mg II	abs.	1.105
	7846.5	[O II]	7.0	1.105
				$\bar{z} = 1.105$
Galaxy 3b	5185	[O II]	0.5	0.391
	6964	[O III]	0.4	0.391
				$\bar{z} = 0.391$

Table 4. Break Amplitudes.

Object	$B(2640)$	$B(2900)$	$R_{UV}$	$B - V$	Notes
F0V	1.69	1.24	1.90	0.31	<i>IUE</i>
F2-3V	1.69	1.19	2.27	0.36	<i>IUE</i>
F5V	2.04	1.23	3.86	0.43	<i>IUE</i>
F6V	2.42	1.33	5.46	0.45	<i>IUE</i>
F7V	2.38	1.34	6.38	0.48	<i>IUE</i>
F9V	2.42	1.47	8.50	0.57	<i>IUE</i>
G0V	2.73	1.59	15.88	0.59	<i>IUE</i>
G2V	2.63	1.70	24.59	0.63	<i>IUE</i>
G5V	2.51	1.97	35.70	0.66	<i>IUE</i>
G8V	2.61	2.13	34.32	0.74	<i>IUE</i>
M32	2.02	1.59	5.49		<i>IUE</i>
NGC 3610	2.02	1.62	19.08		<i>HST</i>
LBDS 53W091	$2.27 \pm 0.35$	$1.70 \pm 0.26$	$3.94 \pm 0.52$		Keck

Table 5. Yale Isochrone Ages ( $Y = 0.2$ )

$Z$	Age (Gyr)	Age (Gyr)
	$B - V = 0.45$	$B - V = 0.60$
0.004	7.4	20.3
0.01	4.4	10.4
0.02 <sup>†</sup>	2.5	5.1
0.04	1.8	3.5
0.1	1.5	2.6

<sup>†</sup>Interpolated from neighbouring metallicities.

Note. — The metallicity of the Sun is  $Z_{\odot} \equiv 0.02$  by definition for the Revised Yale Isochrones.

Table 6. Evolutionary Model Ages: LBDS 53W091

Model	$B(2640)$	$B(2900)$	$R_{UV}$	$R - K$	Mean Age
<i>IUE</i>	$\gtrsim 2.5$	5.1	$\gtrsim 2.5$	...	$\gtrsim 3.4$
Jimenez-MS	$4.2^{+1.0}_{-1.0}$	$6.5^{+2.4}_{-1.6}$	$3.3^{+0.2}_{-0.3}$	$4.6^{+0.4}_{-0.2}$	4.7
BC95	$6.5^{+4.5}_{-4.5}$	$6.0_{-3.5}$	$1.3^{+0.1}_{-0.1}$	$1.2^{+0.2}_{-0.1}$	3.8
Jimenez-full	$3.8^{+1.2}_{-1.1}$	$6.6^{+3.1}_{-2.1}$	$2.8^{+0.3}_{-0.3}$	$2.5^{+0.4}_{-0.2}$	3.9
Worthey	$1.5^{+0.6}_{-0.4}$	$4.3^{+2.7}_{-1.3}$	$1.6^{+0.1}_{-0.2}$	$1.2^{+0.2}_{-0.1}$	2.2

Note. — Age ranges estimated from  $1\sigma$  errors of LBDS measurements.

Table 7. Evolutionary Model Ages: M32

Model	$B(2640)$	$B(2900)$	$R_{UV}$	Mean Age
<i>IUE</i>	$\gtrsim 2.5$	5.1	$\gtrsim 2.5$	$\gtrsim 3.4$
Jimenez–MS	3.5	5.8	4.1	4.5
BC95	3.5	4.0	1.3	2.9
Jimenez–full	3.0	5.8	3.7	4.2
Worthey	1.3	3.2	2.0	2.2

Table 8. Confirmed Blue Stragglers in Open Clusters.

Cluster	Age (Gyr)	Blue Stragglers	References
NGC 6939	1.6	$\geq 1$	a
NGC 2360	1.9	$\geq 1$	a
NGC 7789	2	$\geq 7$	a
NGC 752	2.4	1	a
NGC 2420	4	$\geq 2$	a
NGC 2682 (M67)	5	$\geq 10$	a,b
NGC 188	6	$\sim 11$	c

References. — a: Milone & Latham 1994; b: Montgomery et al. 1993; c: Dinescu et al. 1996

old nearby elliptical galaxy, with dynamical signs of past merger activity, and a spectrum slightly stronger-lined than M32. LBDS 53W091 is slightly bluer, indicating a slightly younger age. The horizontal lines indicate the spectral ranges which we use to define the break amplitudes  $B(2640)$  and  $B(2900)$ , as defined in the text.

Fig. 10.— The fractional contribution of different stellar evolutionary components to the total UV light of an integrated spectrum at an age of 4 Gyr. The model shown is from the synthesis calculations of Jimenez et al. (1996). Note that the main-sequence stars dominate the flux at  $\lambda \lesssim 3500\text{\AA}$ .

Fig. 11.—  $B(2640)$  break amplitude plotted against  $(B - V)$  for main-sequence stars observed by *IUE*. The solid triangles represent individual stars, and the solid squares are measured from average spectra of stars with similar spectral types. Horizontal lines indicate the value of this break amplitude measured for the galaxies M32 and LBDS 53W091. The large scatter in the strength of this break with spectral type only provides a lower limit to the color of the UV bright population of LBDS 53W091, and implies a main sequence turn-off color of  $(B - V) > 0.4$ .

Fig. 12.—  $B(2900)$  break amplitude plotted against  $(B - V)$  for *IUE* main-sequence stars. The symbols are the same as in Figure 11. Horizontal lines indicate the value of this break amplitude measured for the galaxies M32 and LBDS 53W091. This comparison provides a tighter constraint than the  $B(2640)$  break in the previous figure, and implies that the dominant UV population in LBDS 53W091 has a main sequence turn-off color of  $0.55 < (B - V) < 0.75$ .

Fig. 13.— UV color index  $R_{UV}$  plotted against  $(B - V)$  for *IUE* stars. The symbols are the same as in Figure 11. Horizontal lines indicate the value of this break amplitude measured for the galaxies M32 and LBDS 53W091. The spectrum of LBDS 53W091 is consistent with a main sequence turn-off color of  $0.45 < (B - V) < 0.55$ , and is therefore consistent with the age estimates determined from the  $B(2640)$  and  $B(2900)$  spectral breaks.

Fig. 14.— Synthetic spectra at ages of 1, 3 and 5 Gyr from the Solar metallicity evolutionary models of Jimenez et al. (1996) compared with the observed spectrum of LBDS 53W091. The upper panel shows the main-sequence models, and the lower panel shows the “full” models of Jimenez (1996) (see text). The flux (in units of  $F_\lambda$ ) is arbitrarily scaled to unity at  $3150\text{\AA}$  for all spectra. Models with ages less than 3 Gyr are inconsistent with LBDS 53W091.

Fig. 15.—  $B(2640)$  (a) and  $B(2900)$  (b) spectral discontinuities for several models, as indicated in the figure. Horizontal lines are the measured break amplitudes for LBDS 53W091 and M32, as labelled, where the formal  $1\sigma$  error on the value for LBDS 53W091 is also indicated. Note the bimodal distribution of model predictions of the break amplitudes: models which use Kurucz theoretical stellar spectra in the UV (Jimenez and Worthey) have break amplitudes which continually rise, while models which use observed *IUE* stars to form the spectral library (BC95 and G&RV) asymptote at a break amplitudes of  $B(2640) \approx 2.2$  and  $B(2900) \approx 1.7$ .

Fig. 16.—  $R-K$  color for several models, as indicated in the figure. The models of Worthey and BC95 imply a very young age for LBDS 53W091, ages which are inconsistent with the UV spectrum of the galaxy. The models of G&RV and the simple main-sequence model, both of which omit AGB stars from the spectral library (though G&RV have red subgiants and giants) imply an age around 4 Gyr for the galaxy.

Fig. 17.— The models of Guideroni and Rocca-Volmerange compared with the observed spectrum of LBDS 53W091. The flux is arbitrarily scaled to unity at 3150Å for all spectra. Models with ages  $\lesssim 3$  Gyr are inconsistent with LBDS 53W091.

Fig. 18.— Constraints on the cosmological parameters  $H_0$ ,  $\Omega_0$ , and  $\Omega_\Lambda$  derived from the age of LBDS 53W091. We plot the age of the Universe at a redshift of  $z = 1.552$  for a range of cosmological parameters. Models in the left panel assume  $\Lambda = 0$ . Models in the right panel assume a flat universe with a cosmological constant, i.e.  $\Omega_0 + \Omega_\Lambda = 1$ . By virtue of LBDS 53W091 being older than 3.5 Gyr at this redshift, the hatched regions of parameter space are forbidden.

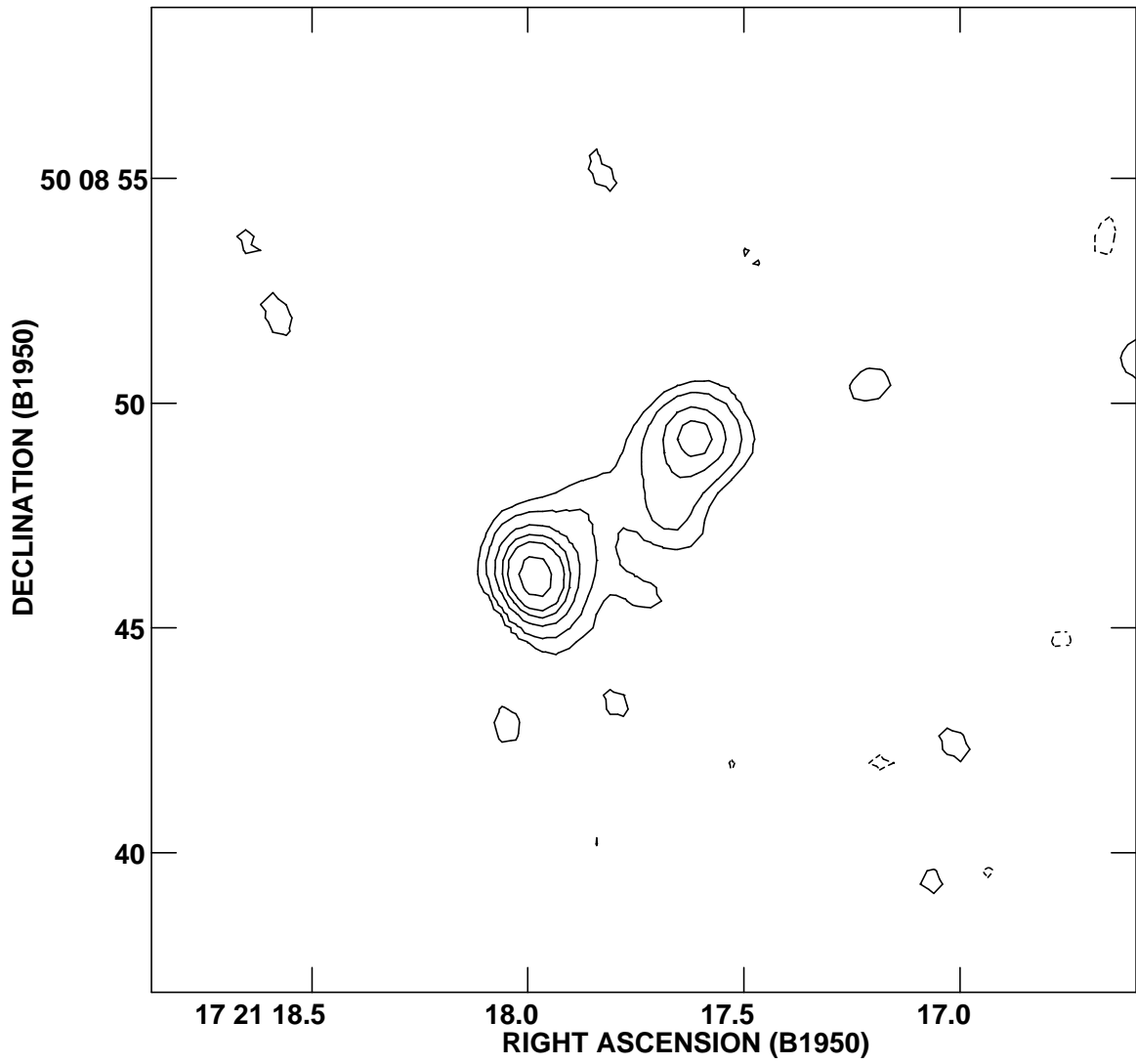


Fig. 1.— VLA A-Array 4.86 GHz map of the radio source LBDS 53W091. The noise in the map is  $\sigma = 52\mu\text{Jy}/\text{beam}$ , and the contours shown are drawn at  $(-3,3,6,12,18,24,36)\sigma$ .

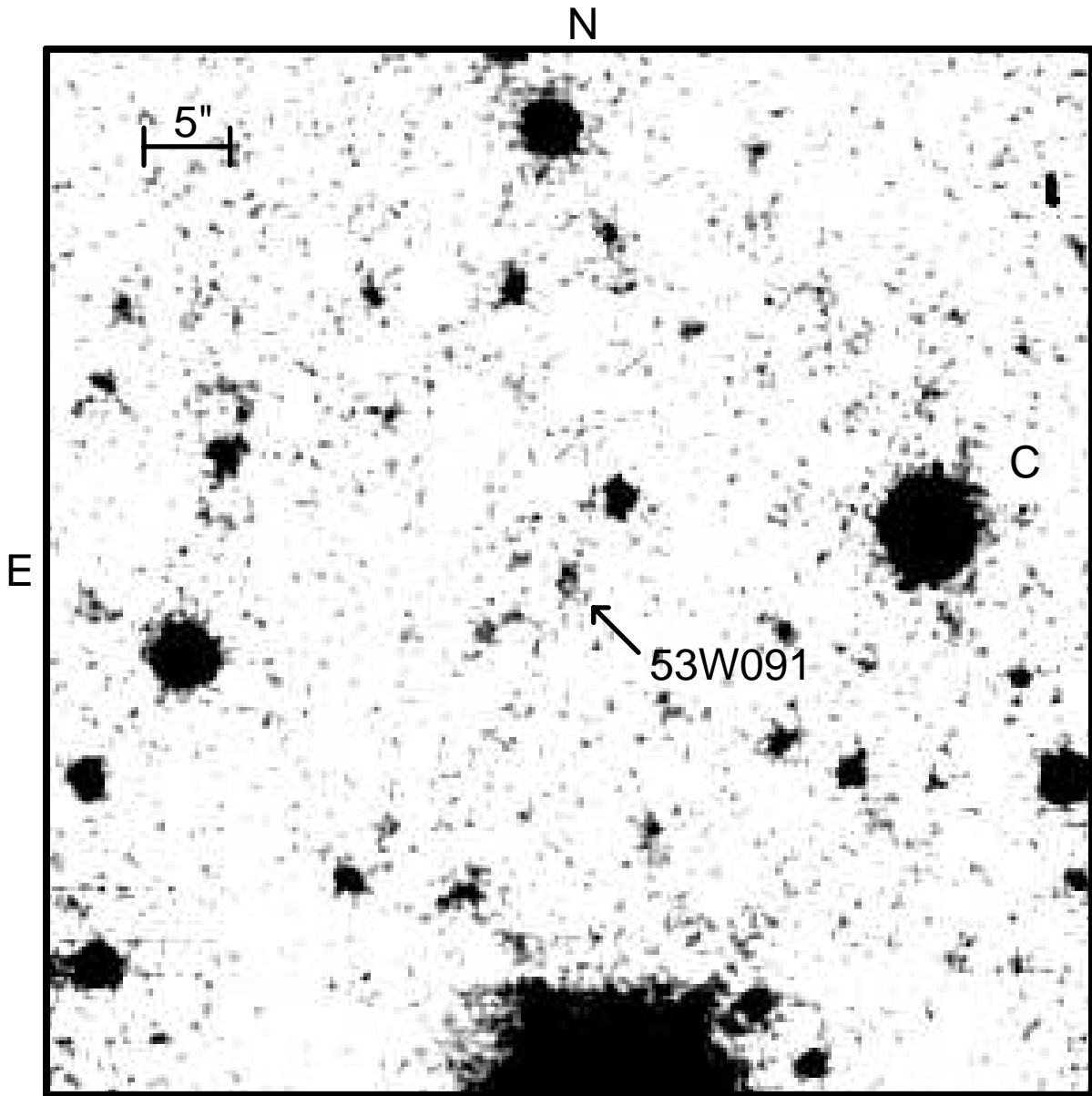


Fig. 2.— Keck  $R$ -band of the field of LBDS 53W091. The frame is  $1'$  on a side; north is to the top and east is to the left. The scale bar shown at top left corresponds to  $\approx 55.7$  kpc at  $z = 1.552$ . The optical counterpart of the radio source is at  $\alpha_{1950} = 17^h 21^m 17^s.78$ ,  $\delta_{1950} = 50^\circ 08' 47''.3$ , and the offset from galaxy C to LBDS 53W091 is  $\Delta\alpha = 20''.5$  (east),  $\Delta\delta = -2''.8$  (south).

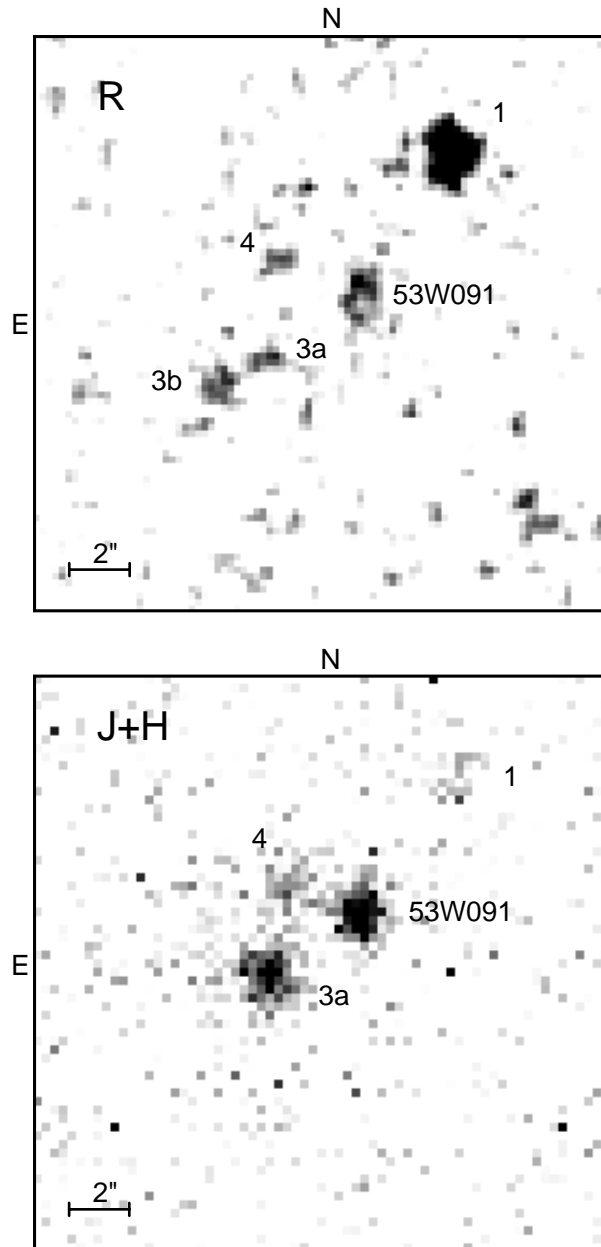


Fig. 3.— (a) Detail of the Keck *R*-band image of LBDS 53W091. (b) Sum of the UKIRT *J* and *H* band images. Both frames are  $19''$  on a side, and north is to the top and east is to the left. The host galaxy of the radio source is labelled 53W091. The blue objects 1 and 3b are foreground emission line galaxies. Object 3a and 4 have similar optical–IR colors to LBDS 53W091 and are likely to be at the same redshift.



Fig. 4.— False color image of the field of LBDS 53W091 constructed using the images in the  $R$ -band (blue),  $J$ -band (green), and  $H$ -band (red) of the field of LBDS 53W091. Note that the host galaxy of the radio source and the two objects nearest it have roughly the same color, and may be all at a common redshift.

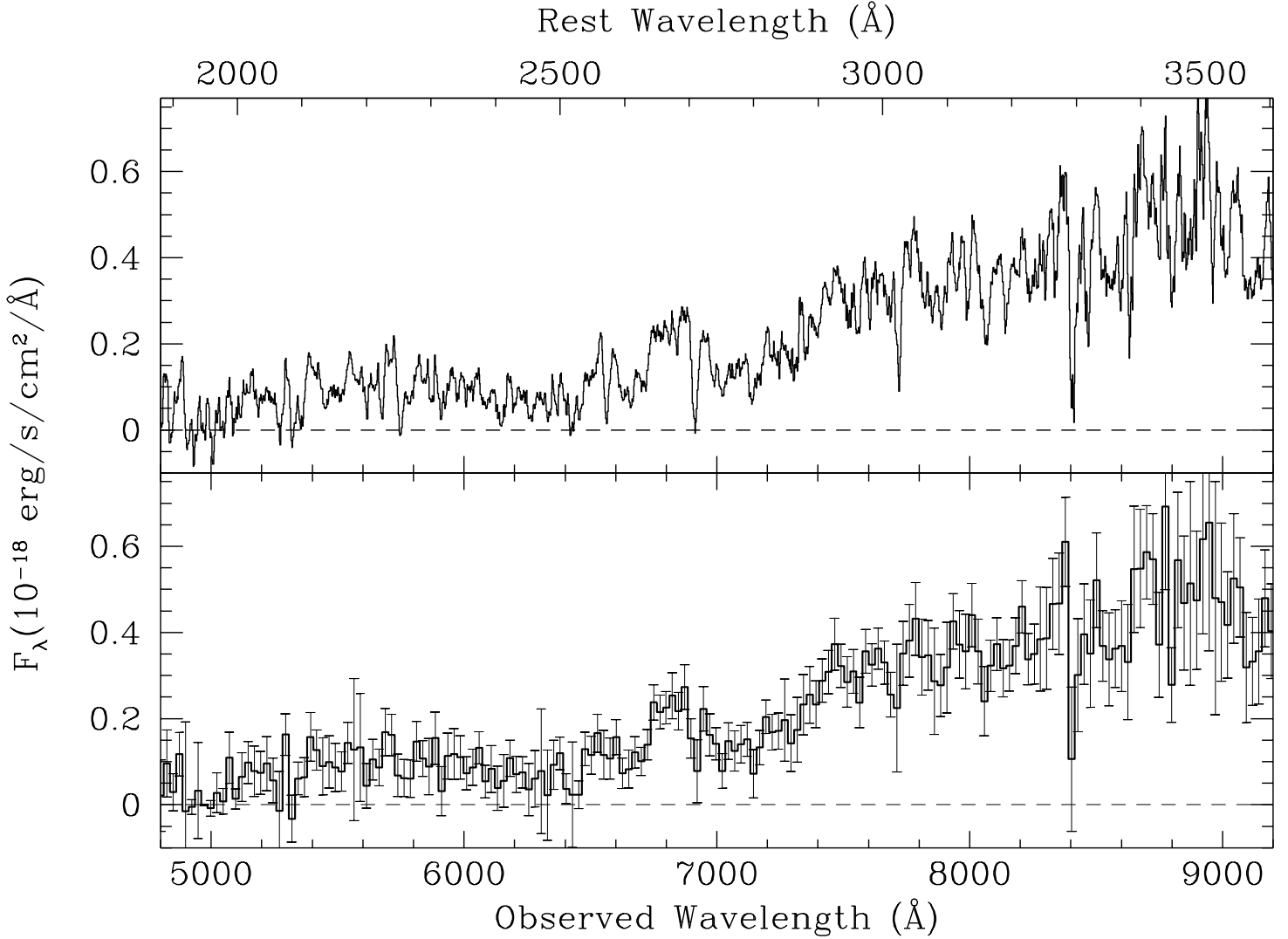


Fig. 5.— The 5.5 hour Keck LRIS spectrum of the host galaxy of LBDS 53W091 plotted in the observers’ frame. The upper panel shows the coadded spectrum smoothed using a boxcar filter of width 9 pixels. The lower panel shows the formal  $1\sigma$  error bars on the spectrum (averaged in 10-pixel bins). The rest wavelength is indicated along the upper abscissa for a redshift of  $z = 1.552$ . The long wavelengths suffer increased noise from atmospheric OH emission lines. The spectrum has been corrected for telluric  $O_2$  absorption in the A- and B-bands.

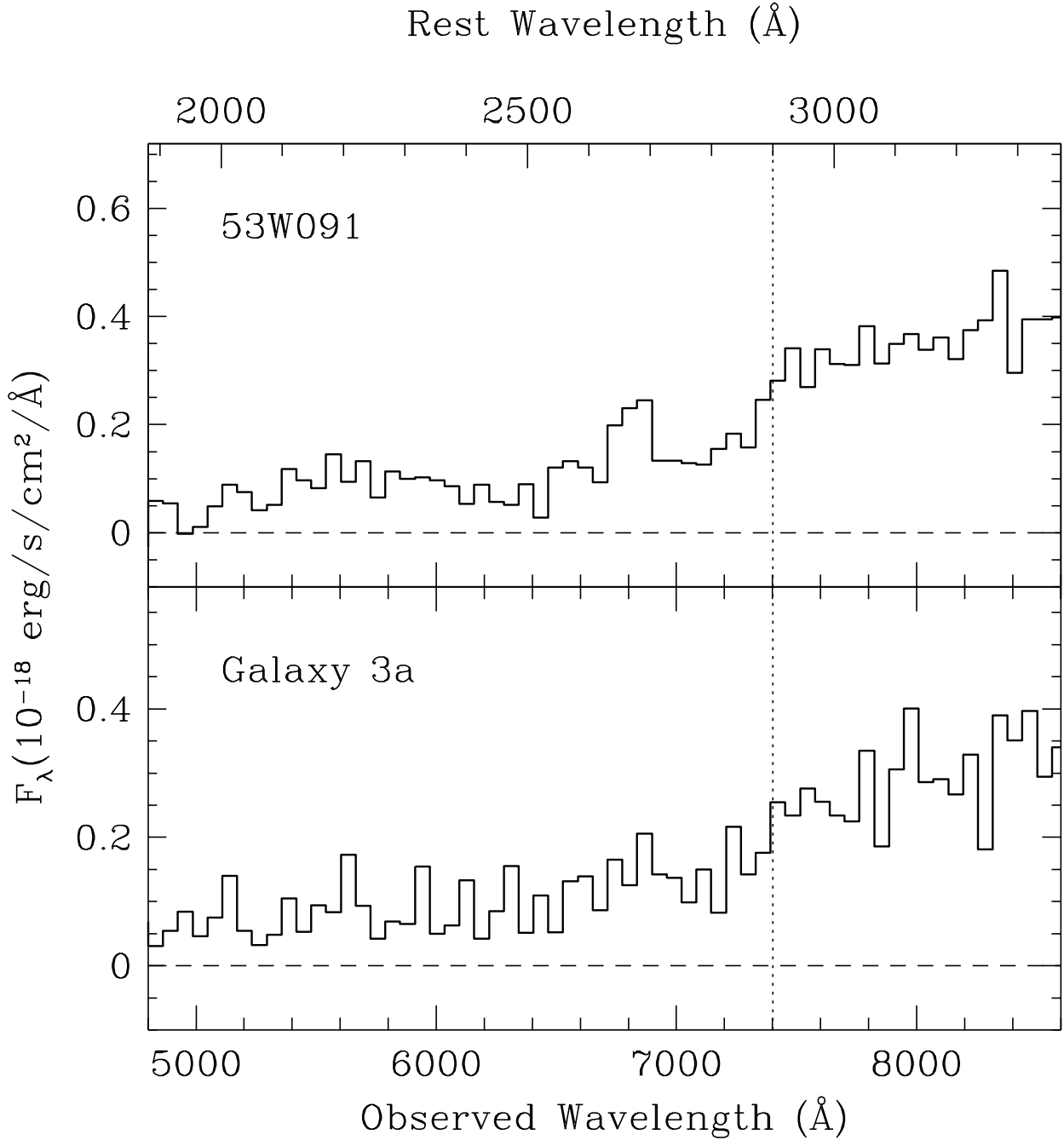


Fig. 6.— Spectra of LBDS 53W091 (shifted) and galaxy 3a plotted in the observers' frame. The spectra have been averaged in 25-pixel bins. The rest wavelength is indicated along the upper abscissa for a redshift of  $z = 1.552$ . The 2900Å discontinuity apparent in both objects. We interpret galaxy 3a to be a faint companion to LBDS 53W091 with both similar age and redshift.

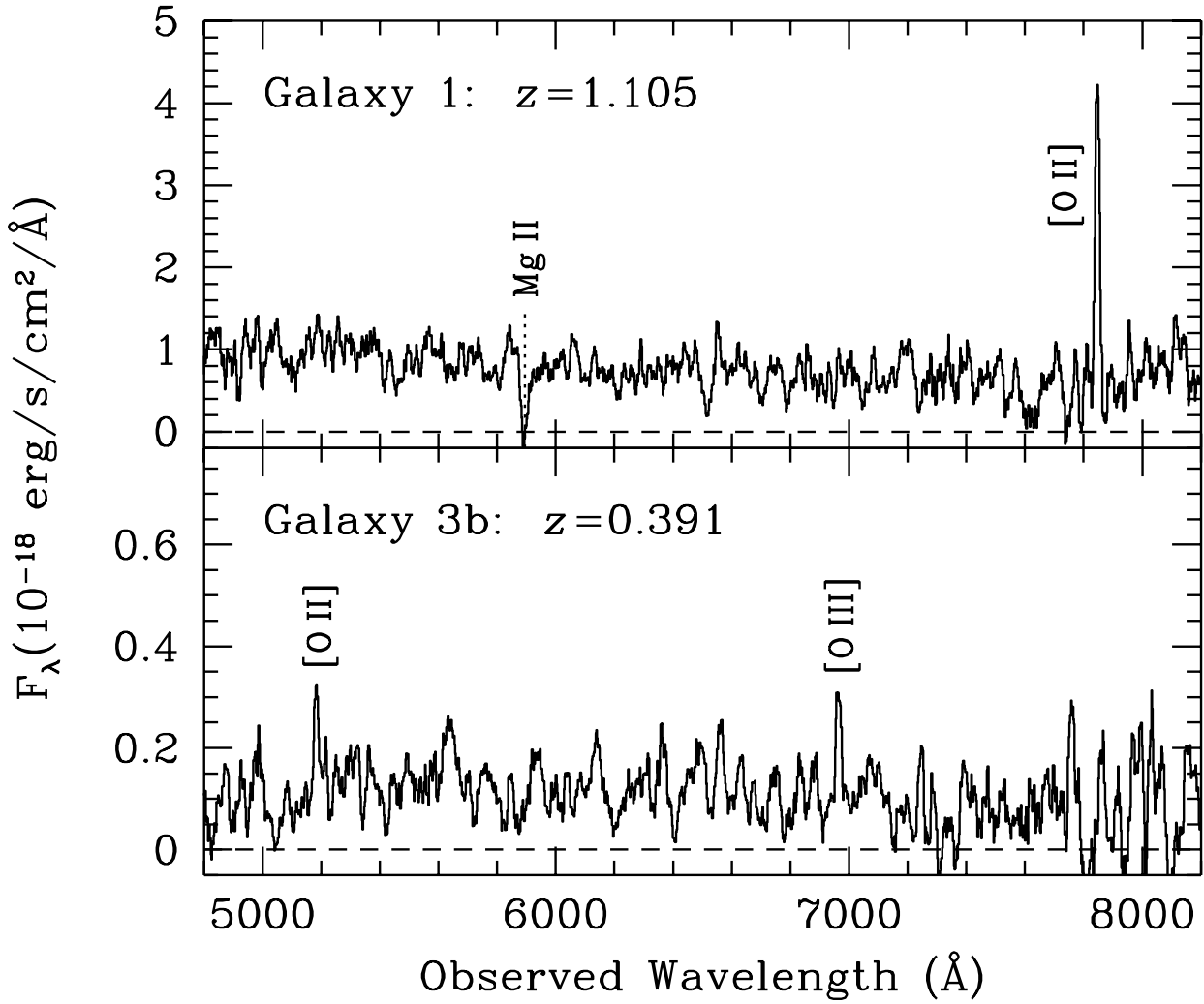


Fig. 7.— Spectra of the blue emission line galaxies labelled “1” (upper panel) and “3b” (lower panel) in Figure 3. The spectra are plotted in the observed frame. The parameters of the emission lines are listed in Table 3.

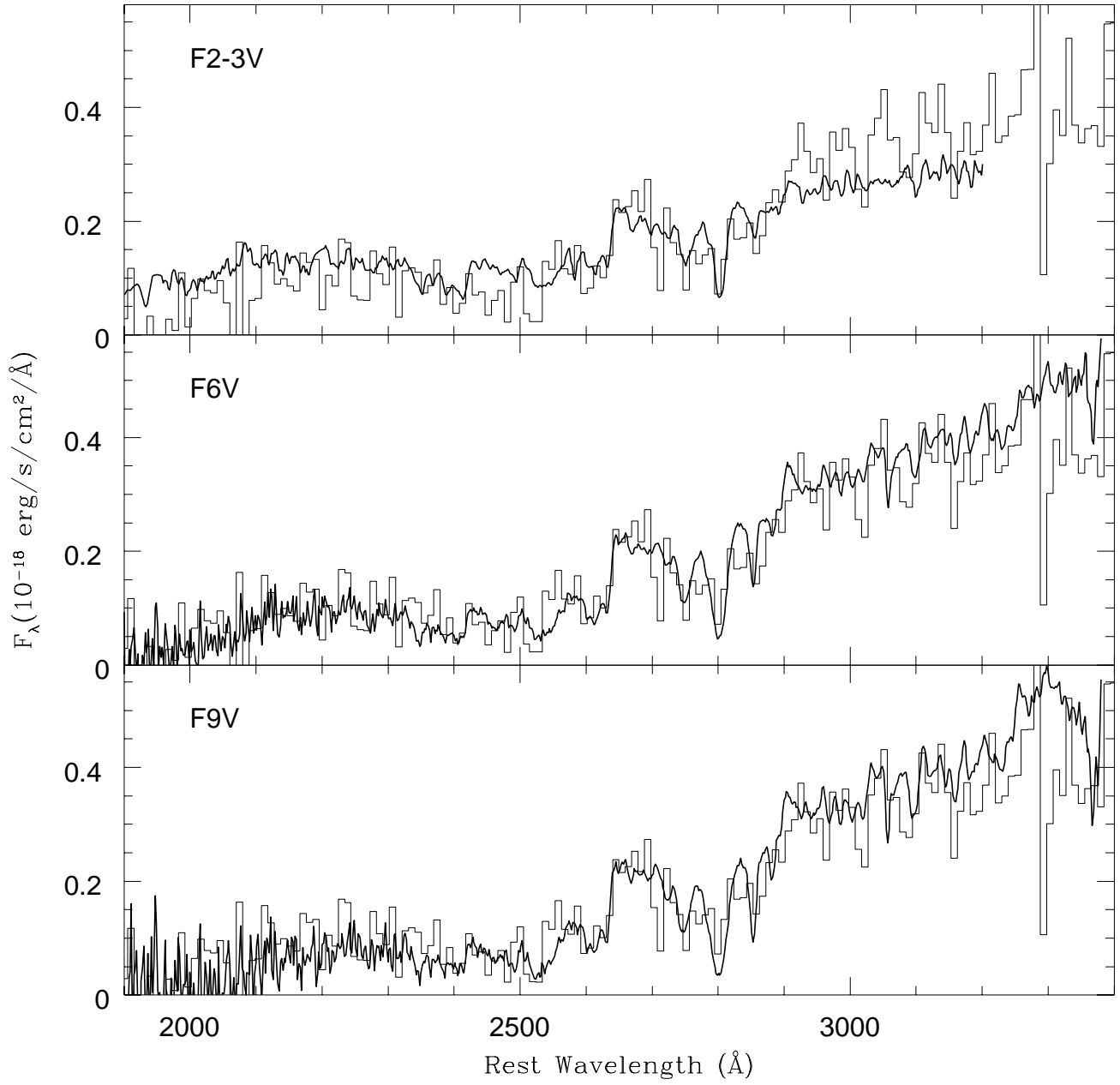


Fig. 8.— Rest frame spectrum of LBDS 53W091 plotted against scaled averages of *IUE* stars. Note that the spectrum of the average F6V stellar type the galaxy spectrum almost perfectly. Assuming Solar metallicity Revised Yale Isochrones, this implies a minimum age just less than 3 Gyr for the bluest turn-off.

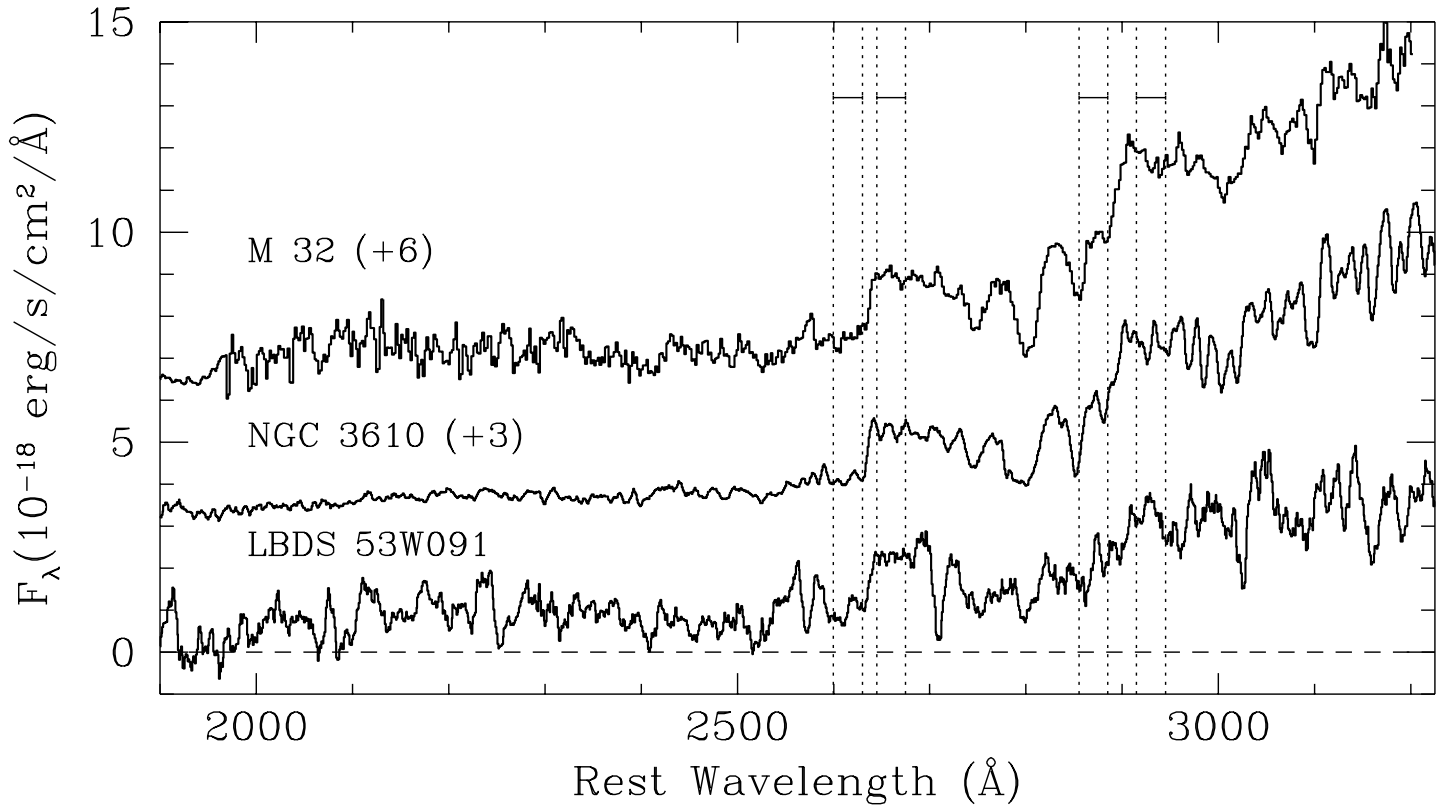


Fig. 9.— Rest frame spectra of LBDS 53W091 (Keck), M32 (*IUE*; Burstein et al. 1988), and NGC 3610 (*HST*; Ferguson, private communication), where the latter two galaxy spectra have been scaled and offset. Note the similarity in the spectral features. NGC 3610 is a moderately old nearby elliptical galaxy, with dynamical signs of past merger activity, and a spectrum slightly stronger-lined than M32. LBDS 53W091 is slightly bluer, indicating a slightly younger age. The horizontal lines indicate the spectral ranges which we use to define the break amplitudes  $B(2640)$  and  $B(2900)$ , as defined in the text.

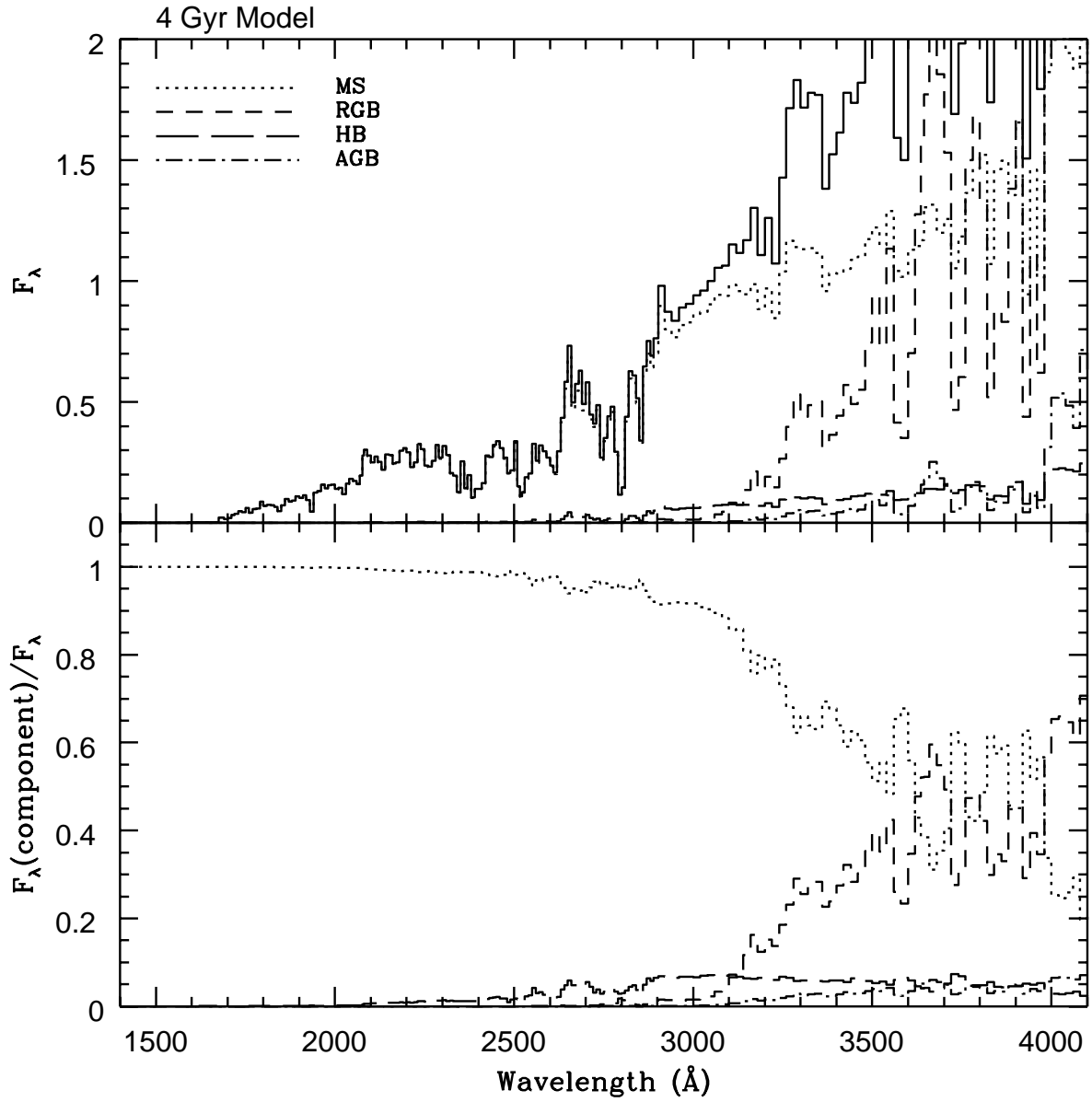


Fig. 10.— The fractional contribution of different stellar evolutionary components to the total UV light of an integrated spectrum at an age of 4 Gyr. The model shown is from the synthesis calculations of Jimenez et al. (1996). Note that the main-sequence stars dominate the flux at  $\lambda \lesssim 3500\text{\AA}$ .

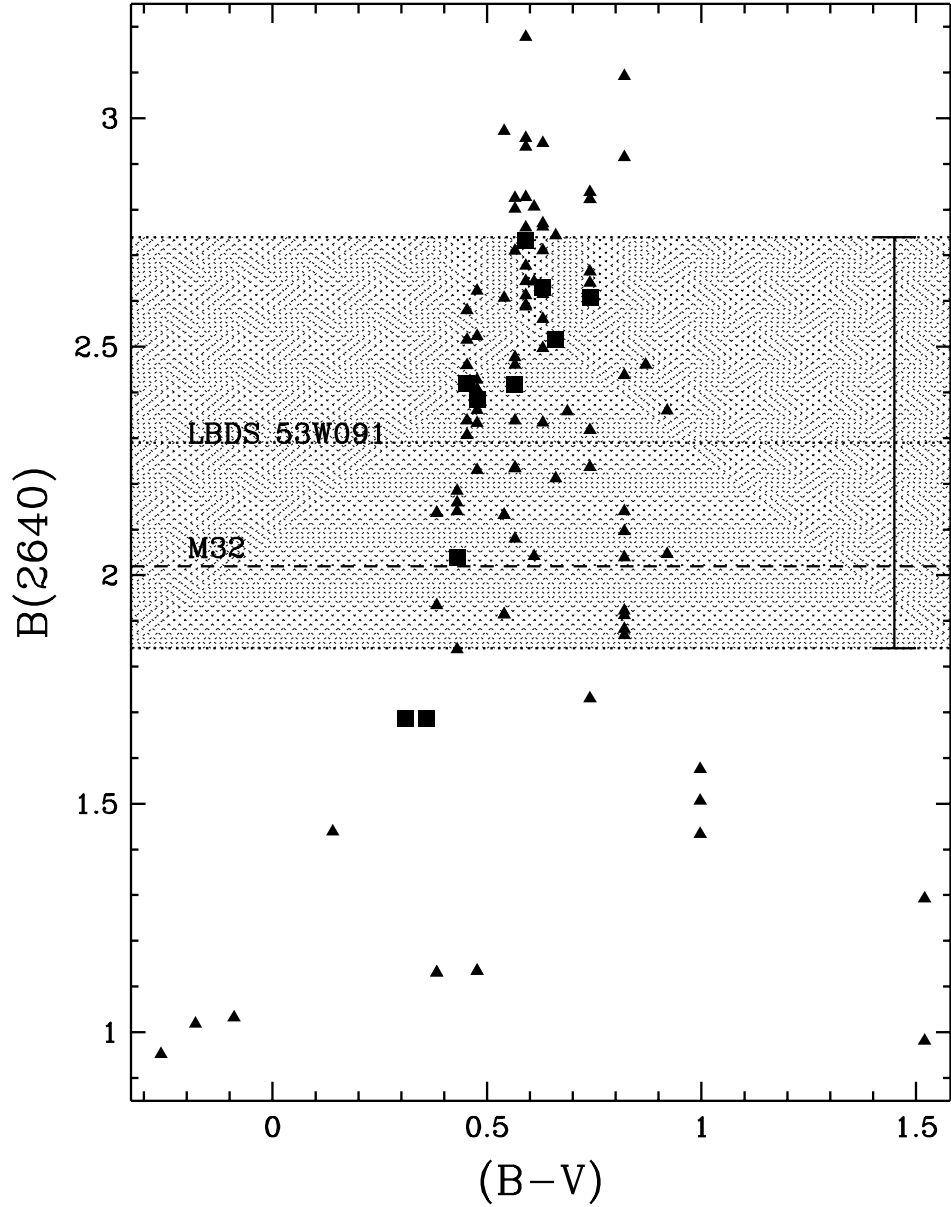


Fig. 11.—  $B(2640)$  break amplitude plotted against  $(B - V)$  for main-sequence stars observed by *IUE*. The solid triangles represent individual stars, and the solid squares are measured from average spectra of stars with similar spectral types. Horizontal lines indicate the value of this break amplitude measured for the galaxies M32 and LBDS 53W091. The large scatter in the strength of this break with spectral type only provides a lower limit to the color of the UV bright population of LBDS 53W091, and implies a main sequence turn-off color of  $(B - V) > 0.4$ .



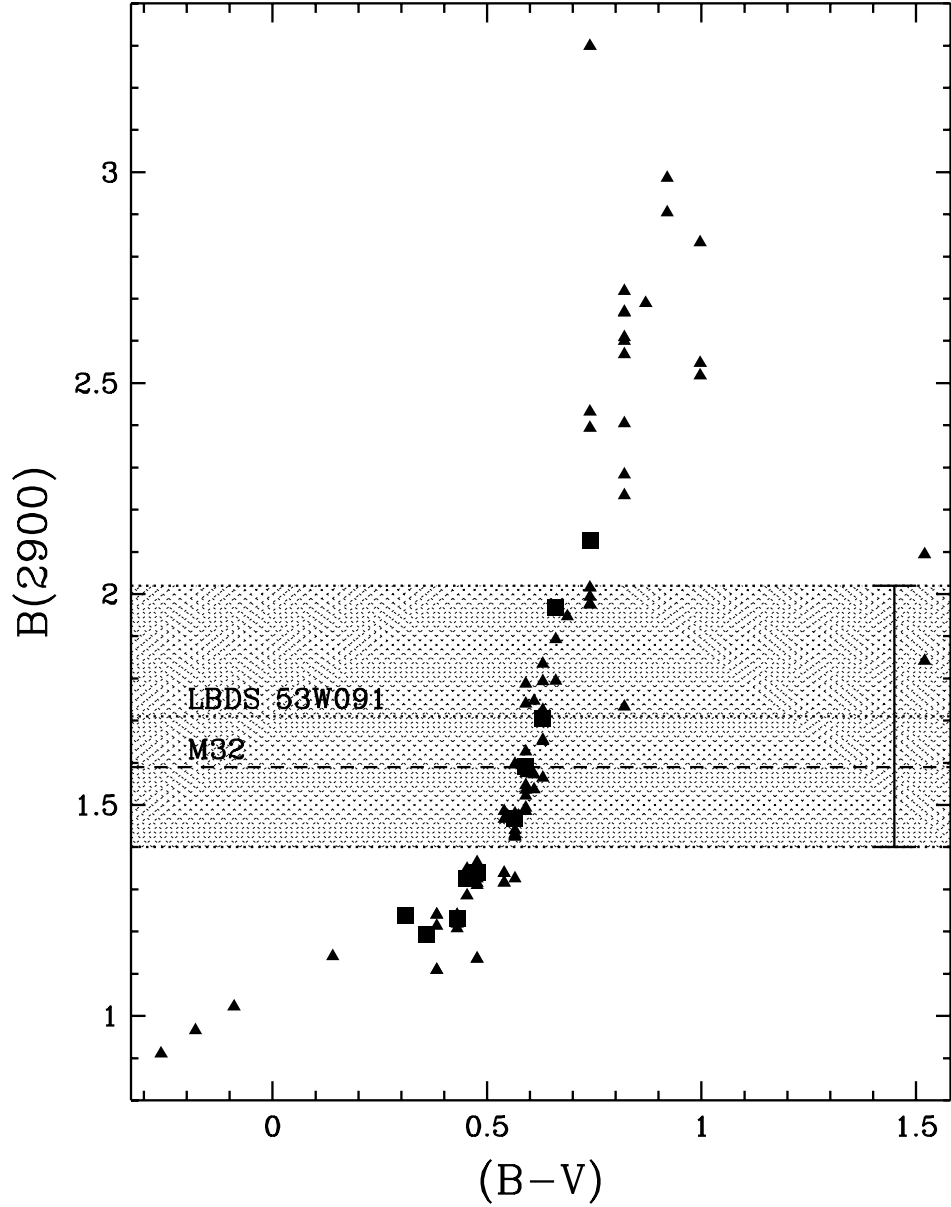


Fig. 12.—  $B(2900)$  break amplitude plotted against  $(B - V)$  for *IUE* main-sequence stars. The symbols are the same as in Figure 11. Horizontal lines indicate the value of this break amplitude measured for the galaxies M32 and LBDS 53W091. This comparison provides a tighter constraint than the  $B(2640)$  break in the previous figure, and implies that the dominant UV population in LBDS 53W091 has a main sequence turn-off color of  $0.55 < (B - V) < 0.75$ .

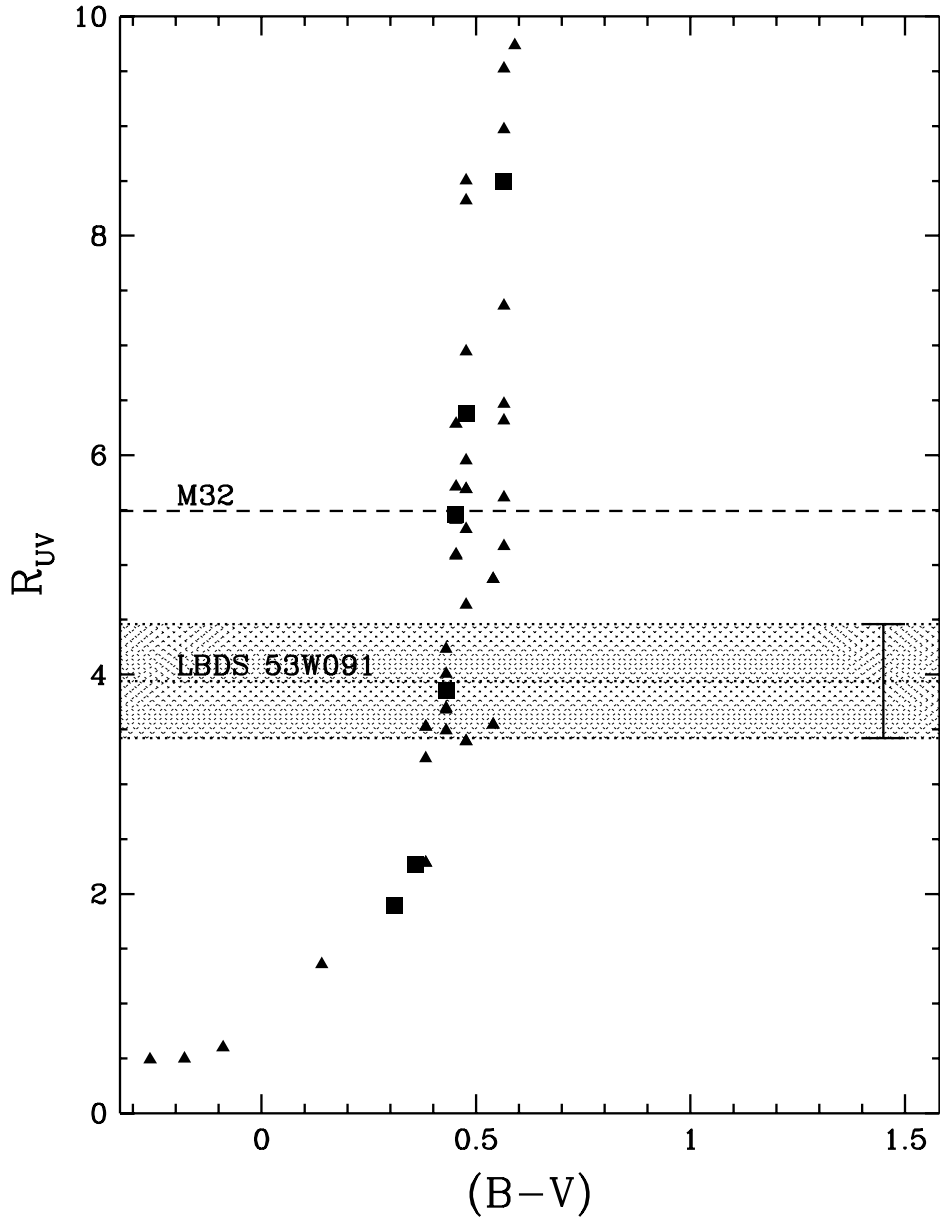


Fig. 13.— UV color index  $R_{UV}$  plotted against  $(B - V)$  for *IUE* stars. The symbols are the same as in Figure 11. Horizontal lines indicate the value of this break amplitude measured for the galaxies M32 and LBDS 53W091. The spectrum of LBDS 53W091 is consistent with a main sequence turn-off color of  $0.45 < (B - V) < 0.55$ , and is therefore consistent with the age estimates determined from the  $B(2640)$  and  $B(2900)$  spectral breaks.

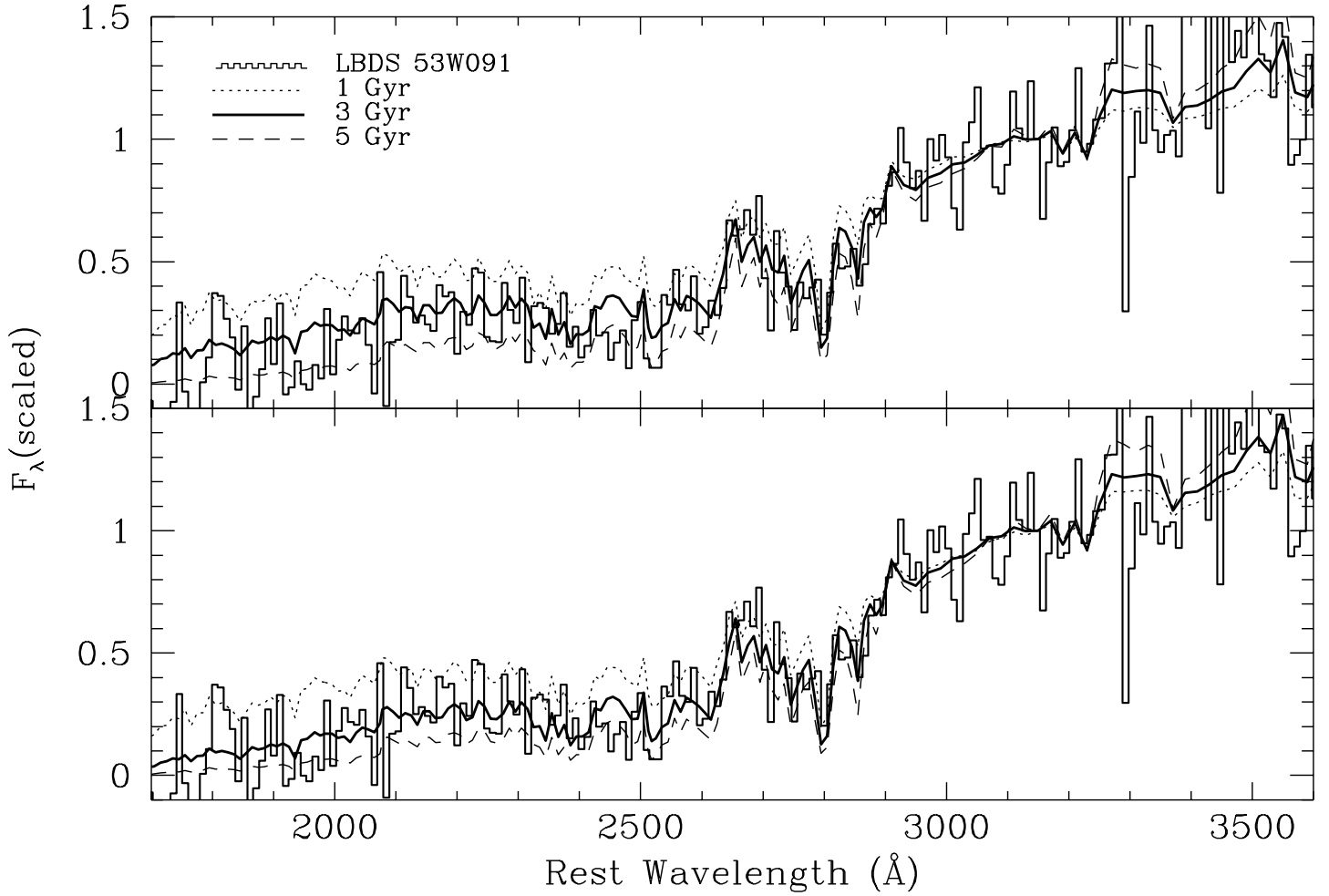


Fig. 14.— Synthetic spectra at ages of 1, 3 and 5 Gyr from the Solar metallicity evolutionary models of Jimenez et al. (1996) compared with the observed spectrum of LBDS 53W091. The upper panel shows the main–sequence models, and the lower panel shows the “full” models of Jimenez (1996) (see text). The flux (in units of  $F_\lambda$ ) is arbitrarily scaled to unity at  $3150\text{\AA}$  for all spectra. Models with ages less than 3 Gyr are inconsistent with LBDS 53W091.

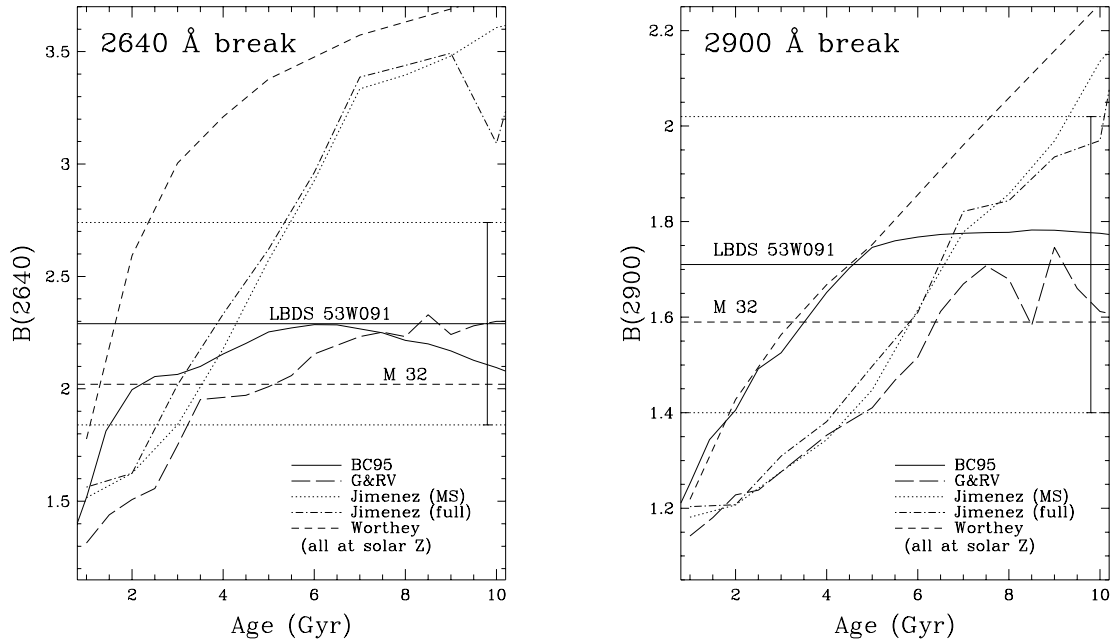


Fig. 15.—  $B(2640)$  (a) and  $B(2900)$  (b) spectral discontinuities for several models, as indicated in the figure. Horizontal lines are the measured break amplitudes for LBDS 53W091 and M32, as labelled, where the formal  $1\sigma$  error on the value for LBDS 53W091 is also indicated. Note the bimodal distribution of model predictions of the break amplitudes: models which use Kurucz theoretical stellar spectra in the UV (Jimenez and Worthey) have break amplitudes which continually rise, while models which use observed *IUE* stars to form the spectral library (BC95 and G&RV) asymptote at a break amplitudes of  $B(2640) \approx 2.2$  and  $B(2900) \approx 1.7$ .

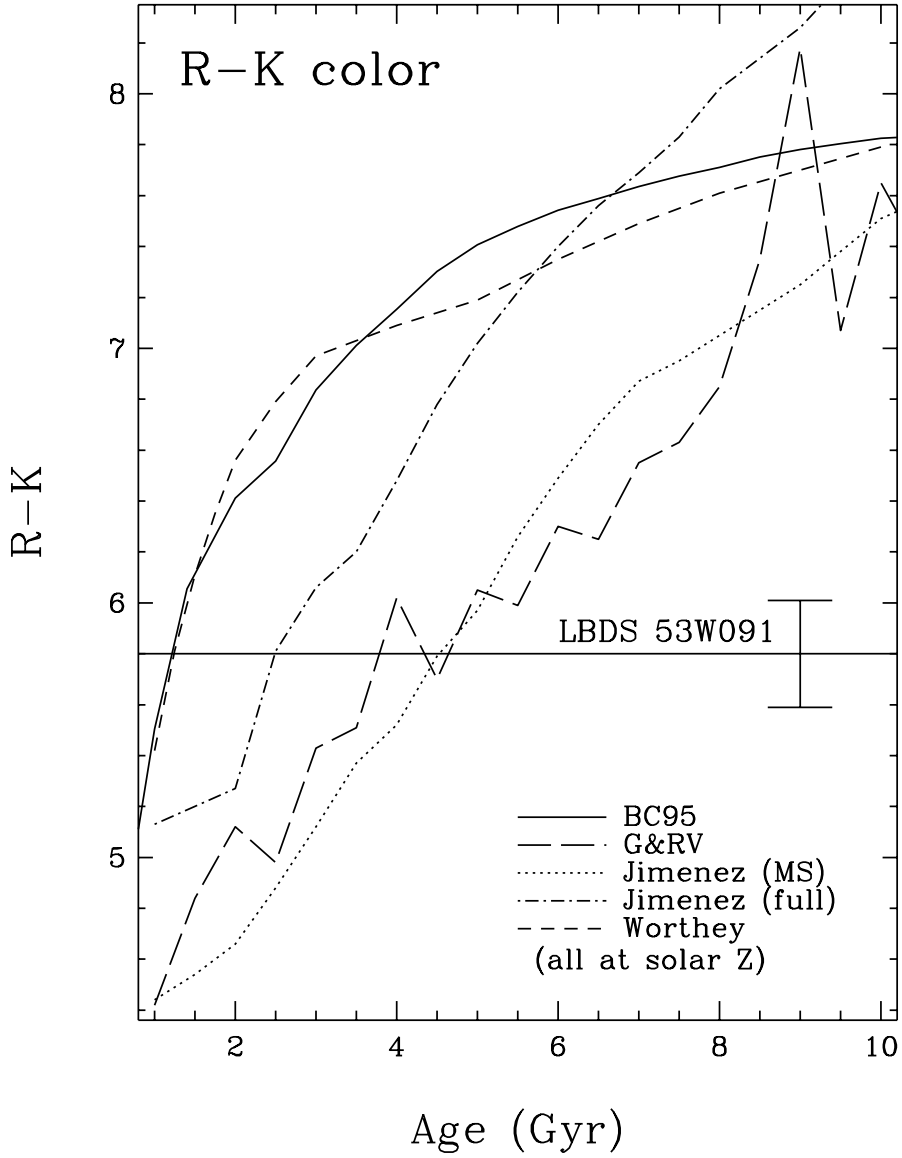


Fig. 16.—  $R-K$  color for several models, as indicated in the figure. The models of Worthey and BC95 imply a very young age for LBDS 53W091, ages which are inconsistent with the UV spectrum of the galaxy. The models of G&RV and the simple main-sequence model, both of which omit AGB stars from the spectral library (though G&RV have red subgiants and giants) imply an age around 4 Gyr for the galaxy.

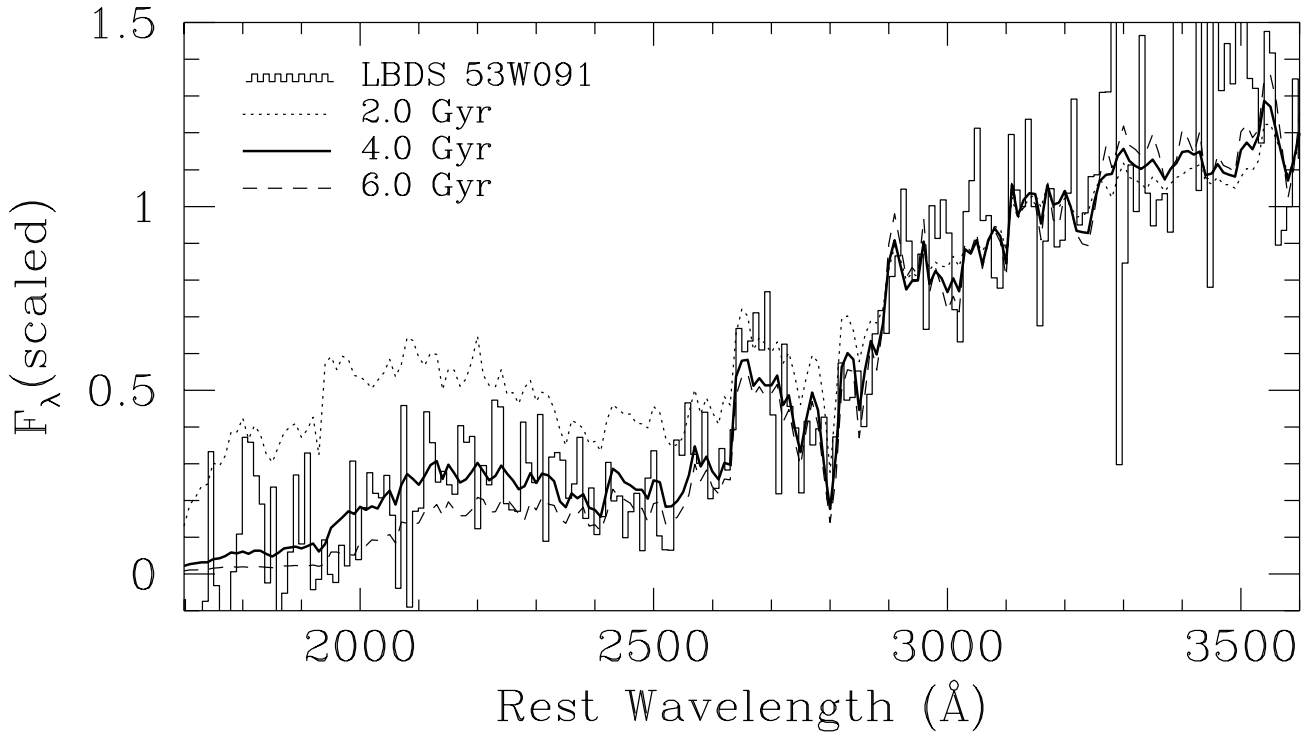


Fig. 17.— The models of Guideroni and Rocca–Volmerange compared with the observed spectrum of LBDS 53W091. The flux is arbitrarily scaled to unity at  $3150\text{\AA}$  for all spectra. Models with ages  $\lesssim 3$  Gyr are inconsistent with LBDS 53W091.

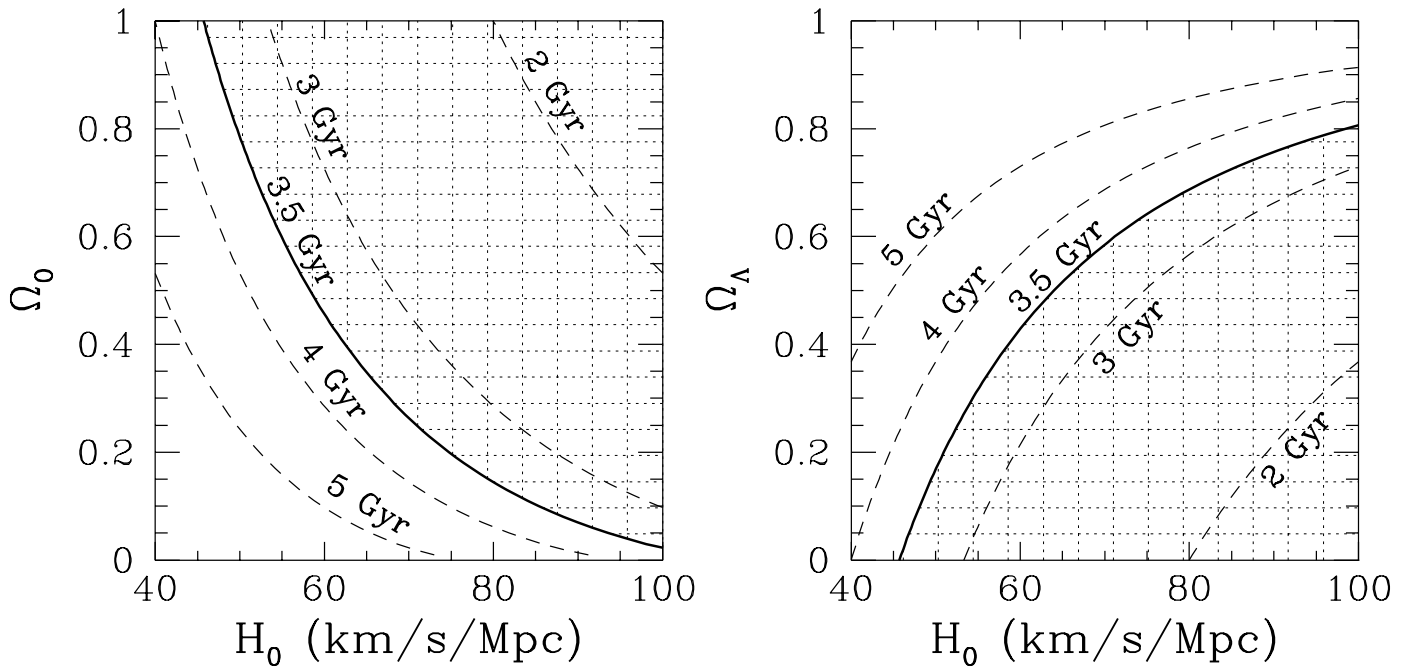


Fig. 18.— Constraints on the cosmological parameters  $H_0$ ,  $\Omega_0$ , and  $\Omega_\Lambda$  derived from the age of LBDS 53W091. We plot the age of the Universe at a redshift of  $z = 1.552$  for a range of cosmological parameters. Models in the left panel assume  $\Lambda = 0$ . Models in the right panel assume a flat universe with a cosmological constant, i.e.  $\Omega_0 + \Omega_\Lambda = 1$ . By virtue of LBDS 53W091 being older than 3.5 Gyr at this redshift, the hatched regions of parameter space are forbidden.

Table 1. Radio Data<sup>†</sup>

Component	$RA_{1950}$	$DEC_{1950}$	$\nu$ (GHz)	$F_\nu$ (mJy)
Total	$17^h21^m17^s81 \pm 0^s01$	$+50^\circ08'47''6 \pm 0''1$	1.565	$23.0 \pm 1.7$
			4.860	$6.5 \pm 0.4$
SE Lobe	$17^h21^m17^s98 \pm 0^s01$	$+50^\circ08'46''18 \pm 0''05$	1.565	$11.5 \pm 1.3$
			4.860	$3.37 \pm 0.23$
NW Lobe	$17^h21^m17^s64 \pm 0^s01$	$+50^\circ08'49''00 \pm 0''07$	1.565	$10.7 \pm 1.3$
			4.860	$2.25 \pm 0.29$

<sup>†</sup>Data in this table are derived from the 1995 VLA observations described in the text.

Table 2. Photometry in the LBDS 53W091 Field.

	Galaxy 1	LBDS 53W091	Galaxy 3a	Galaxy 3b	Galaxy 4
<i>R</i>	$23.9 \pm 0.1$	$24.5 \pm 0.2$	$24.9 \pm 0.2$	$25.1 \pm 0.3$	$25.5 \pm 0.3$
<i>J</i>	$22.1 \pm 0.5$	$20.5 \pm 0.1$	$20.5 \pm 0.1$	$22.2 \pm 0.5$	$20.6 \pm 0.2$
<i>H</i>	$21.5 \pm 0.4$	$19.5 \pm 0.1$	$19.5 \pm 0.1$	$21.5 \pm 0.4$	$20.0 \pm 0.1$
<i>K</i>	$19.8 \pm 0.3$	$18.7 \pm 0.1$	$18.9 \pm 0.2$	$20.1 \pm 0.5$	$19.0 \pm 0.3$

Note. — All magnitudes are measured in a  $4''$  diameter aperture.



Table 3. Line Identifications in the Blue Galaxies.

Source	$\lambda_{\text{obs}}$ Å	Line ID	Flux ( $10^{-17}$ erg cm $^{-2}$ s $^{-1}$ )	$z$
Galaxy 1	5897:	Mg II	abs.	1.105
	7846.5	[O II]	7.0	1.105
				$\bar{z} = 1.105$
Galaxy 3b	5185	[O II]	0.5	0.391
	6964	[O III]	0.4	0.391
				$\bar{z} = 0.391$

Table 4. Break Amplitudes.

Object	$B(2640)$	$B(2900)$	$R_{UV}$	$B - V$	Notes
F0V	1.69	1.24	1.90	0.31	<i>IUE</i>
F2-3V	1.69	1.19	2.27	0.36	<i>IUE</i>
F5V	2.04	1.23	3.86	0.43	<i>IUE</i>
F6V	2.42	1.33	5.46	0.45	<i>IUE</i>
F7V	2.38	1.34	6.38	0.48	<i>IUE</i>
F9V	2.42	1.47	8.50	0.57	<i>IUE</i>
G0V	2.73	1.59	15.88	0.59	<i>IUE</i>
G2V	2.63	1.70	24.59	0.63	<i>IUE</i>
G5V	2.51	1.97	35.70	0.66	<i>IUE</i>
G8V	2.61	2.13	34.32	0.74	<i>IUE</i>
M32	2.02	1.59	5.49		<i>IUE</i>
NGC 3610	2.02	1.62	19.08		<i>HST</i>
LBDS 53W091	$2.27 \pm 0.35$	$1.70 \pm 0.26$	$3.94 \pm 0.52$		Keck

Table 5. Yale Isochrone Ages ( $Y = 0.2$ )

$Z$	Age (Gyr)	
	$B - V = 0.45$	$B - V = 0.60$
0.004	7.4	20.3
0.01	4.4	10.4
0.02 <sup>†</sup>	2.5	5.1
0.04	1.8	3.5
0.1	1.5	2.6

<sup>†</sup>Interpolated from neighbouring metallicities.

Note. — The metallicity of the Sun is  $Z_{\odot} \equiv 0.02$  by definition for the Revised Yale Isochrones.

Table 6. Evolutionary Model Ages: LBDS 53W091

Model	$B(2640)$	$B(2900)$	$R_{UV}$	$R - K$	Mean Age
<i>IUE</i>	$\gtrsim 2.5$	5.1	$\gtrsim 2.5$	...	$\gtrsim 3.4$
Jimenez–MS	$4.2^{+1.0}_{-1.0}$	$6.5^{+2.4}_{-1.6}$	$3.3^{+0.2}_{-0.3}$	$4.6^{+0.4}_{-0.2}$	4.7
BC95	$6.5^{+4.5}_{-4.5}$	$6.0_{-3.5}$	$1.3^{+0.1}_{-0.1}$	$1.2^{+0.2}_{-0.1}$	3.8
Jimenez–full	$3.8^{+1.2}_{-1.1}$	$6.6^{+3.1}_{-2.1}$	$2.8^{+0.3}_{-0.3}$	$2.5^{+0.4}_{-0.2}$	3.9
Worthey	$1.5^{+0.6}_{-0.4}$	$4.3^{+2.7}_{-1.3}$	$1.6^{+0.1}_{-0.2}$	$1.2^{+0.2}_{-0.1}$	2.2

Note. — Age ranges estimated from  $1\sigma$  errors of LBDS measurements.

Table 7. Evolutionary Model Ages: M32

Model	$B(2640)$	$B(2900)$	$R_{UV}$	Mean Age
<i>IUE</i>	$\gtrsim 2.5$	5.1	$\gtrsim 2.5$	$\gtrsim 3.4$
Jimenez–MS	3.5	5.8	4.1	4.5
BC95	3.5	4.0	1.3	2.9
Jimenez–full	3.0	5.8	3.7	4.2
Worthey	1.3	3.2	2.0	2.2

Table 8. Confirmed Blue Stragglers in Open Clusters.

Cluster	Age (Gyr)	Blue Stragglers	References
NGC 6939	1.6	$\geq 1$	a
NGC 2360	1.9	$\geq 1$	a
NGC 7789	2	$\geq 7$	a
NGC 752	2.4	1	a
NGC 2420	4	$\geq 2$	a
NGC 2682 (M67)	5	$\geq 10$	a,b
NGC 188	6	$\sim 11$	c

References. — a: Milone & Latham 1994; b: Montgomery et al. 1993; c: Dinescu et al. 1996